Ore Geology Reviews 111 (2019) 102981

Contents lists available at ScienceDirect

Ore Geology Reviews

journal homepage: www.elsevier.com/locate/oregeorev

Black and red alterations associated with the Baimadong uranium deposit (Guizhou, China): Geological and geochemical characteristics and genetic relationship with uranium mineralization

Yanyan Li[a,b], Chengjiang Zhang[a,*], Guoxiang Chi[b], Ji Duo[a,c], Zenghua Li[d], Hao Song[a]

[a] College of Earth Science, Chengdu University of Technology, Chengdu 610059, Sichuan, China
[b] Department of Geology, University of Regina, Regina, Saskatchewan, Canada
[c] Tibet Bureau of Geological Exploration, Lhasa, Tibet 850000, China
[d] East China University of Technology, Nanchang 330013, China

ARTICLE INFO

Keywords:
Carbonaceous-siliceous-pelitic rock-type uranium deposits
Black alteration
Red alteration
Baimadong
SW China

ABSTRACT

The Baimadong uranium deposit is hosted in carbonate rocks that were subjected to extensive black and red alterations, silicification and argillization, and is assigned to the carbonaceous-siliceous-pelitic rock-type uranium deposits in the Chinese literature. However, the nature of the mineralization, especially the black and red alterations and their relationship with uranium mineralization, remains poorly understood. Petrographic and Raman spectroscopic studies indicate that the black material are organic matter mainly composed of graphite and bitumen, whereas the red-altered rocks are characterized by abundant iron oxides. Crosscutting relationships suggest that the black alteration occurred before the red alteration. Comparison of whole-rock geochemistry between the different types of rocks suggests that total organic carbon (TOC), U and total organic sulfur (TOS) were gained through the black alteration, and FeO^T was gained through the red alteration, whereas total inorganic carbon (TIC), CaO and MgO were lost in both types of alterations. The $\delta^{13}C_{org}$ (PDB) values and biomarker characteristics of the black-altered rocks suggest that the organic matter was derived from the black shale of the Niutitang Formation underneath the deposit. U enrichment is associated with both the black and red alterations, and shows positive correlations with Al_2O_3, K_2O, TiO_2, SiO_2, TOC and TOS. It is proposed that the uranium mineralization at Baimadong resulted from superposition of two fluid events controlled by a common structural system. First, petroleum generated in the black shales of the Niutitang Formation and hydrothermal fluids migrated along cross-formational faults to the carbonate rocks of the Qingxudong and Shilengshui formations, causing the black alteration and preliminary uranium enrichment. Second, an oxidizing, U-bearing fluid flowed through the same structure and precipitated uraninite through reaction with the black-altered rocks, accompanied by precipitation of hematite and goethite as marked by the red alteration. The combination of black and red alterations with major faults may be used as a mineralization indicator in the exploration of this type of U deposits.

1. Introduction

The uranium deposits in China have been classified into four main types, i.e., sandstone-type, volcanic-type, granite-type, and carbonaceous-siliceous-pelitic rock-type (Huang et al., 1994; Min, 1995; Hu et al., 2008). Among these types, the carbonaceous-siliceous-pelitic rock-type, hereinafter referred to as CSP-type, is least understood by the international uranium geoscience community in terms of its geological characteristics and genesis, in part because the name is used exclusively in the Chinese literature and the meaning of 'carbonaceous' is ambiguous. The host rocks of this type of uranium deposits include a variety of non-metamorphic to weakly metamorphic carbonaceous-siliceous-pelitic carbonate rocks (including limestones and dolostones) and pelitic rocks (including slates and shales), and the mineralization appears to be controlled by a combination of lithologies and cross-cutting structures (Zhang, 1982; Liu, 1989; Huang et al., 1994; Min, 1995; Hu et al., 2008). Therefore, some of the CSP-type uranium deposits may belong to the category of black shale uranium deposits in the IAEA classification (IAEA, 2009, 2018), and some of them may be classified as the carbonate-hosted deposits in the new IAEA (2018)

* Corresponding author.
E-mail address: zcj@cdut.edu.cn (C. Zhang).

https://doi.org/10.1016/j.oregeorev.2019.102981
Received 27 December 2018; Received in revised form 30 May 2019; Accepted 14 June 2019
Available online 15 June 2019

classification. In the case of black shale uranium deposits, the organic matter in the black shales is clearly of syn-sedimentary to burial diagenetic origin, whereas in the case of carbonate-hosted uranium deposits, the organic matter in the host rocks is likely imported from external sources (IAEA, 2018).

In this paper, we examine one of the more important carbonate-hosted CSP-type uranium deposits, the Baimadong uranium deposit in Guizhou Province of South China, in order to gain a better understanding of the geological characteristics and genesis of this type of uranium deposits, in particular the nature of black-colored and red-colored alterations associated with mineralization and its role in uranium mineralization. Detailed petrographic studies were carried out for samples from different parts of the deposit, and representative altered and least altered rocks were sampled for major and trace elements analysis. Organic matter was examined with Raman spectroscopy and analyzed for carbon isotopes, chloroform asphalt "A", biomarkers (m/z85, m/z191, m/z217) and group components. The whole-rock geochemical data were used to estimate the elements gained and lost during the mineralization and alterations, and the organic geochemical data were used to trace the origin of the organic matter.

2. Geologic setting and local geology

2.1. Regional geologic setting

The Baimadong area is located in Kaiyang County, central Guizhou Province (Qianzhong), southwestern China (Fig. 1a). This area is situated in the Guiyang complex tectonic deformation zone in the Qianzhong uplift, which is located within the Yangtze platform (Guizhou Bureau of Geology and Minerals, 1987; Long et al., 2017). The Yangtze platform is surrounded by an early Paleozoic fold belt in southeastern Guizhou (Qiandongnan) and a Mesozoic fold belt in southern Guizhou (Qiannan) (Guizhou Bureau of Geology and Minerals, 1987). The basement of the Yangtze platform is made of metamorphosed shallow marine sedimentary rocks of Meso- to Neoproterozoic ages, which experienced two major tectonic movements, i.e., the Wuling Movement (ca. 820 Ma; Dai et al., 2010) and the Xuefeng Movement (ca. 760 Ma; Zhang, 1995). The cover of the platform is composed of dominantly marine sedimentary rocks of Neoproterozoic (Sinian) to Triassic ages and terrestrial sedimentary rocks since Jurassic, which were subject to multiple tectono-thermal events during the Phanerozoic as discussed below.

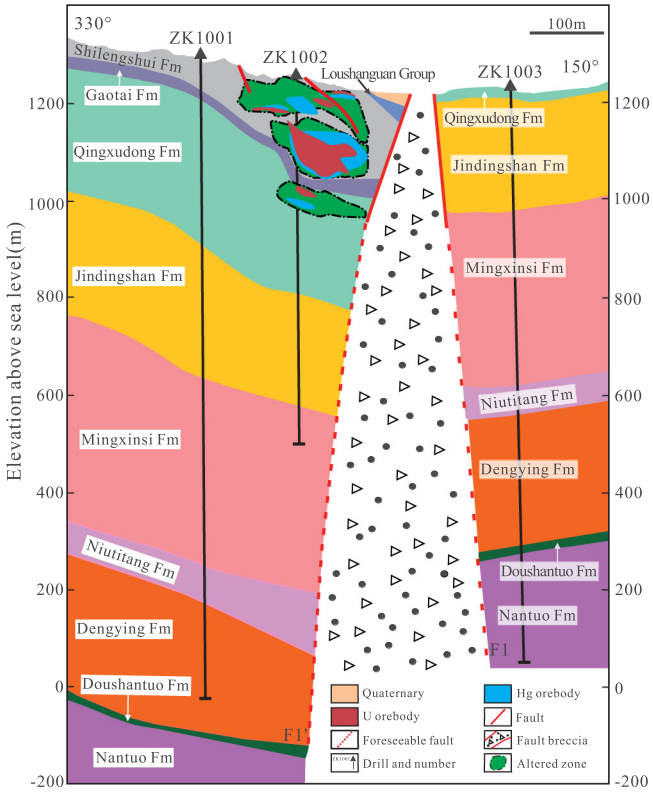

Fig. 2. A cross section of the Baimadong uranium deposit (see Fig. 1b for location).

The central Guizhou region experienced a transgression-regression cycle from Sinian to Late Cambrian, when the Yunan Movement

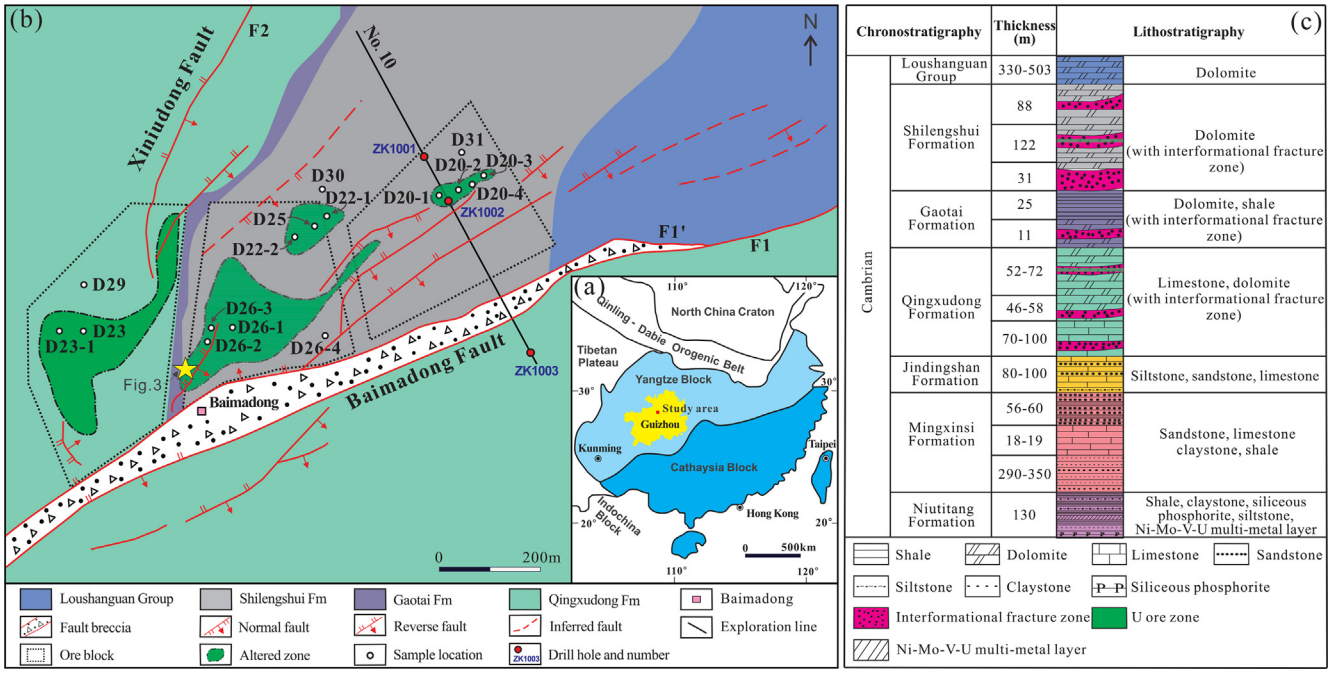

Fig. 1. (a) Regional map showing the tectonic setting of SW China and location of the study area (modified from Zhou et al., 2014). (b) Geological map of the Baimadong uranium mining district (modified from Mo et al., 2016). (c) The stratigraphic column of the Baimadong area.

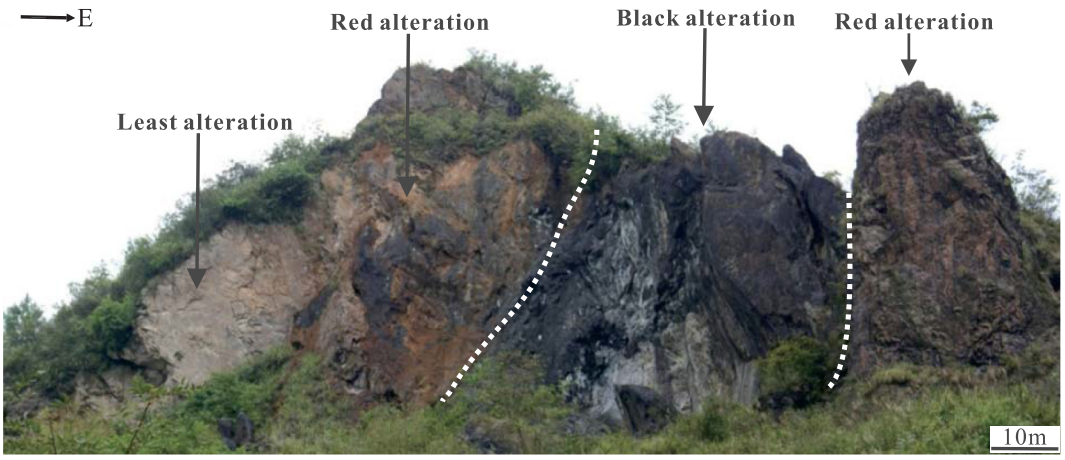

Fig. 3. An outcrop showing the relationships between the black-altered, red-altered and least altered rocks in the Baimadong area (see Fig. 1b for location).

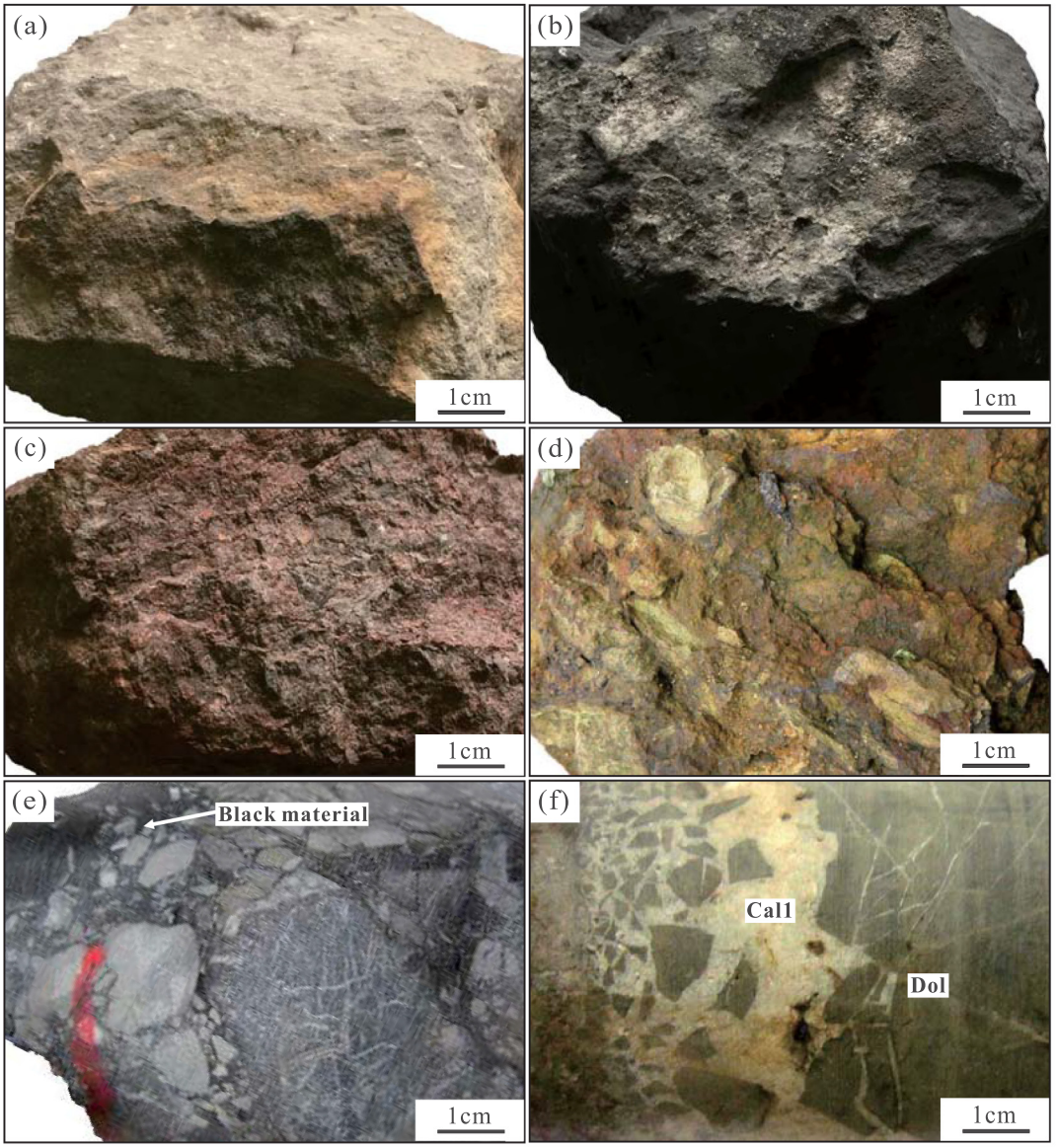

Fig. 4. Hand samples of least altered rock (a), black-altered rock (b), red-altered rock (c), red-altered rock with remnant black-altered rock (d), breccia with black material in the matrix (e), and breccia cemented by calcite (f).

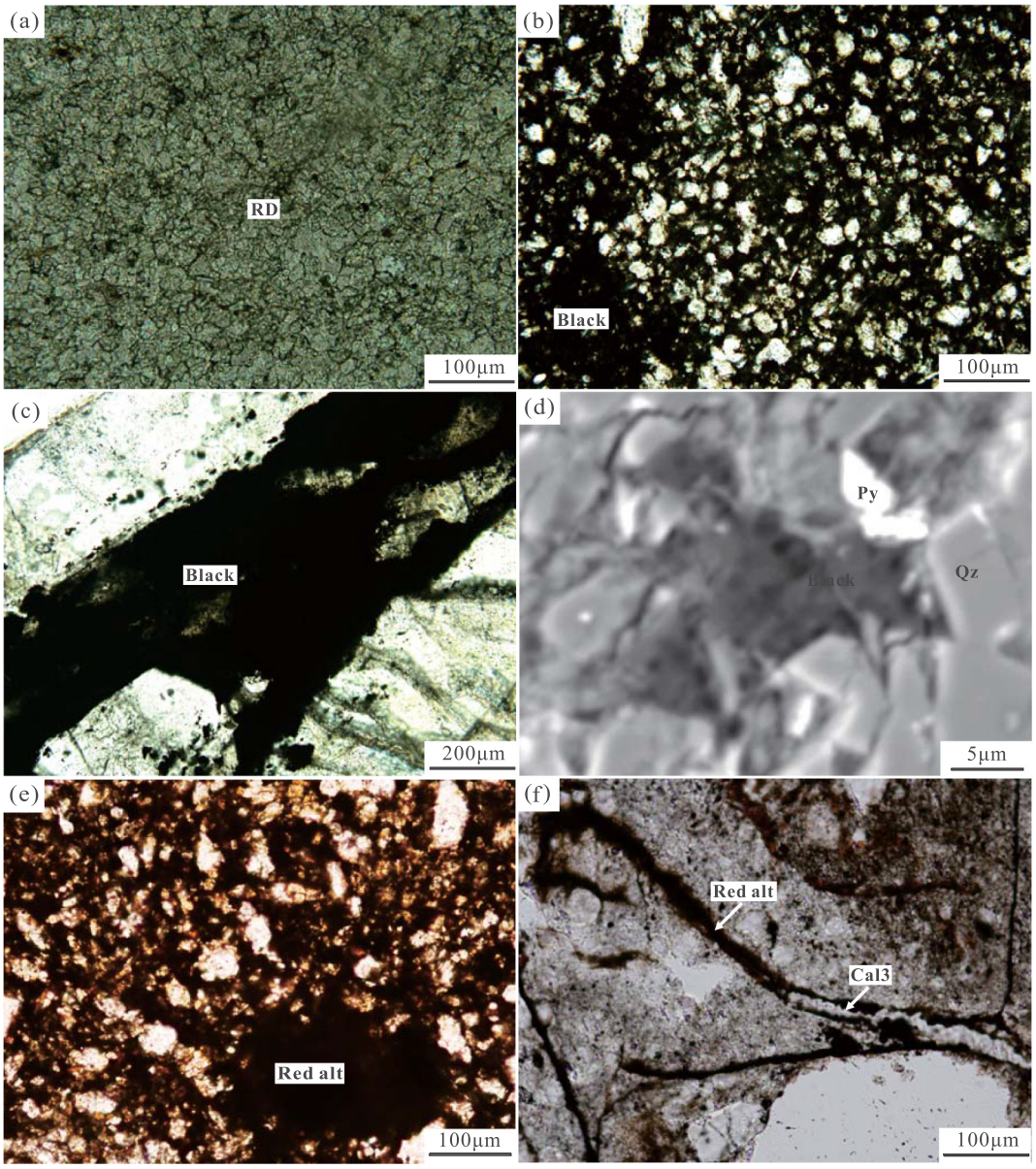

Fig. 5. Photomicrographs and SEM image showing petrographic features of least altered, black-altered, red-altered rocks: replacement dolomite (RD) in least altered rock (a), black material filling interstitial space (b) and fractures (c) in black-altered rocks, authigenic quartz with well-developed crystal shape in black-altered rock (d), and reddish material fills interstitial space (e) and fractures (f).

resulted in the Qianzhong uplift (Guizhou Bureau of Geology and Minerals, 1987; Mei et al., 2005; Long et al., 2017). The subsequent Duyun Movement (ca. 458 Ma) and Guangxi Movement (ca. 443 Ma) further uplifted central Guizhou and resulted in variable degrees of denudation of the marine sedimentary rocks deposited during Ordovician and Early Silurian (Yu et al., 1995). After more than 100 million years of weathering and erosion, the region received marine sedimentation again in early Carboniferous (Guizhou Bureau of Geology and Minerals, 1987; Liu, 2001; Ling et al., 2015; Long et al., 2017), and was then uplifted again due to the Ziyun Movement in Late Carboniferous.

The region was subsequently affected by the Dongwu Movement (between Middle and Late Permian) and the associated Emeishan mantle-plume related basalt eruption event (He et al., 2005). These were followed by the Indosinian Movement (Late Triassic), with intervening marine and terrestrial sedimentation in Middle Permian and Lower Triassic, and then by the Yanshanian (end of Middle Jurassic) and Himalayan (Late Cretaceous) movements (Huang, 1945; Guizhou Bureau of Geology and Minerals, 1987; Wang and Mo, 1995; Chen, 2005). These tectonic movements resulted in strong folding and faulting of the strata in the Qiandongnan and Qiannan fold belts, and affected the strata in the Qianzhong uplift within the Yangtze Platform to variable degrees.

2.2. Geology of the Baimadong deposit

The strata outcropping in the Baimadong area are all Cambrian, including (from bottom to top) the Niutitang, Mingxinsi, Jindingshan, Qingxudong, Gaotai and Shilengshui formations and the Loushanguan Group (Fig. 1c). The Niutitang Formation consists of black shale enriched in organic matter and pyrite, with intercalated phosphatic nodule, siliceous phosphorite, carbonaceous claystone and siltstone, and Ni-Mo-V-U-rich layers. The Mingxinsi Formation is composed of claystone intercalated with sandstone, limestone, and sandstone intercalated with shale. The Jindingshan Formation comprises siltstone, sandstone and limestone. The Qingxudong Formation consists of

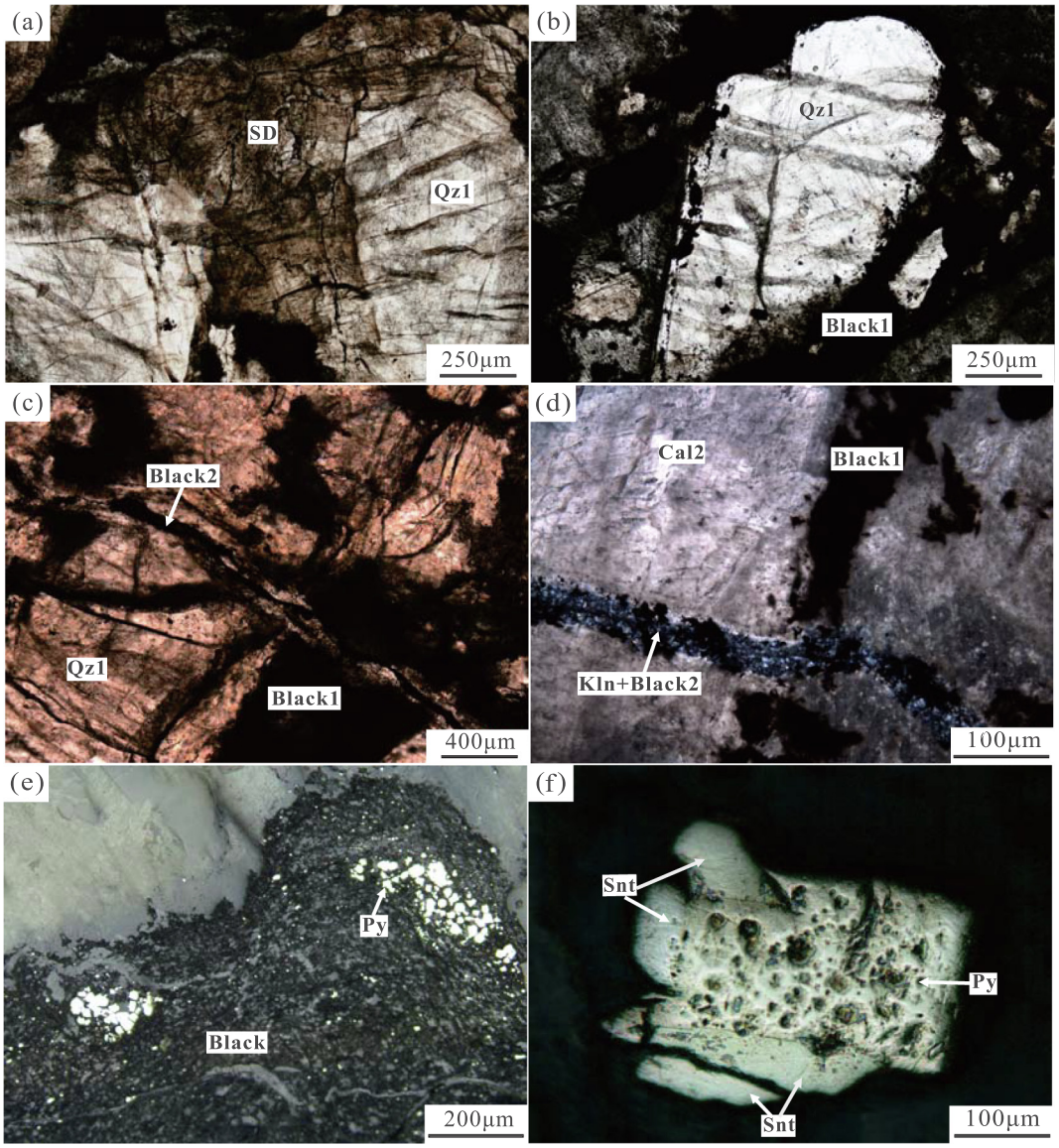

Fig. 6. Photomicrographs showing coarse saddle dolomite (SD) replaced by coarse-grained quartz (Qz1) (a), black material (Black 1) crosscutting coarse crystal quartz (Qz1) (b), a second generation of black material (Black 2) crosscutting Black 1 (c), Black 2 associated with kaolinite (Kln) crosscutting Black 1 (d), pyrite (Py) occurring in black material (e), and stibnite (Snt) coexisting with pyrite (Py) (f).

limestone and dolomite, and the Gaotai Formation is composed of dolomite and shale. The Shilengshui Formation and the Loushanguan Group comprise mainly dolomite (Chen, 1990; Pi et al., 2013; Yang et al., 2013; Yi and Zhao, 2014; Long et al., 2017).

The strata in the Baimadong area are folded and faulted. The Baimadong fault (F1) is ~50 km long, ENE-trending and dipping to SE at angles of 75° to nearly 90° (Fig. 1b). The Xiniudong fault (F2) is ~8 km long, NNE-trending and dipping to SE at angles of 15–30° (Fig. 1b). The F1 fault is characterized by a breccia zone of up to > 100 m width (Figs. 1b and 2), with angular to subangular fragments of the host rocks cemented by calcite, quartz as well as black material (organic matter) (Fig. 4e and f). Several smaller-scale, NNE- to ENE-trending and SE-dipping faults are developed between F1 and F2 (Fig. 1b). The strata strike NE and dip to SE, and secondary folds are locally developed near F1. Multiple interformational fracture zones are developed within the Qingxudong, Gaotai and Shilengshui formations (Fig. 1c).

The uranium mineralization is hosted in altered rocks in the interformational fracture zones in the Qingxudong (the lower ore zone) and Shilengshui (the upper ore zone) formations adjacent to the F1 fault (Chen, 1990) (Figs. 1b, c and 2). The ores are best developed in the black-altered rocks that are overprinted by red alteration. The lower ore zone consists of lenticular and cap-shaped orebodies that are 30–80 m (up to 350 m) long and 2–10 m thick, with average grades of 0.10–0.21% U (up to 0.60%). The upper ore zone consists of lenticular, saclike and crescent-shaped orebodies that are 7–35 m (up to 60 m) long and 2–10 m thick, with average grades of 0.06–0.11% U (up to 0.20%). The U orebodies are closely associated with mercury mineralization in both the lower and upper ore zones (Fig. 2), with average grades of 0.02–0.25% Hg (up to 0.60%) (Huang and Zheng, 2016; Zhang et al., 2017).

The main wall rock alterations associated with mineralization include black alteration, red alteration, silicification and argillization. The black alteration, characterized by enrichment of organic matter responsible for the black color (Fig. 3), is the most prominent feature in the breccia zone along the F1 fault; whereas the red alteration, characterized by development of Fe oxides causing the reddish color, overprinted the black alteration (Fig. 3) and is closely related to U mineralization. Uranium is present as micron-sized grains of uraninite and adsorption (Chen, 1990). Other metallic minerals include pyrite,

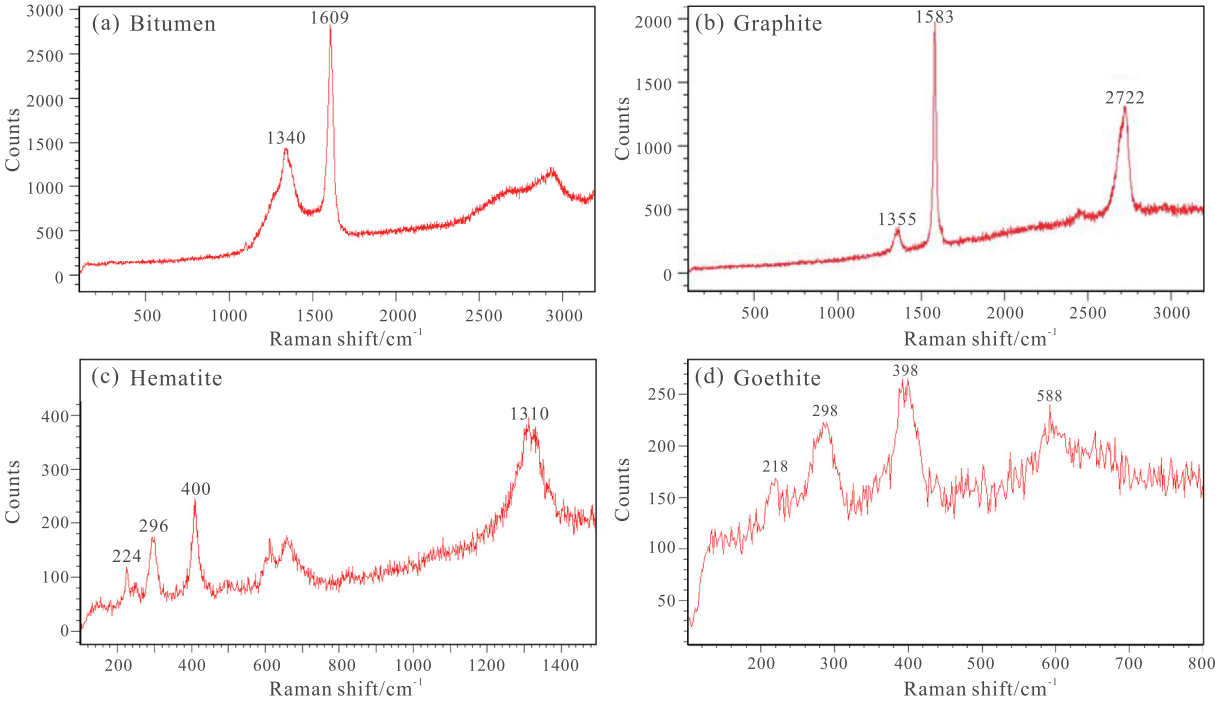

Fig. 7. Raman spectra of bitumen (a), graphite (b), hematite (c), and goethite (d).

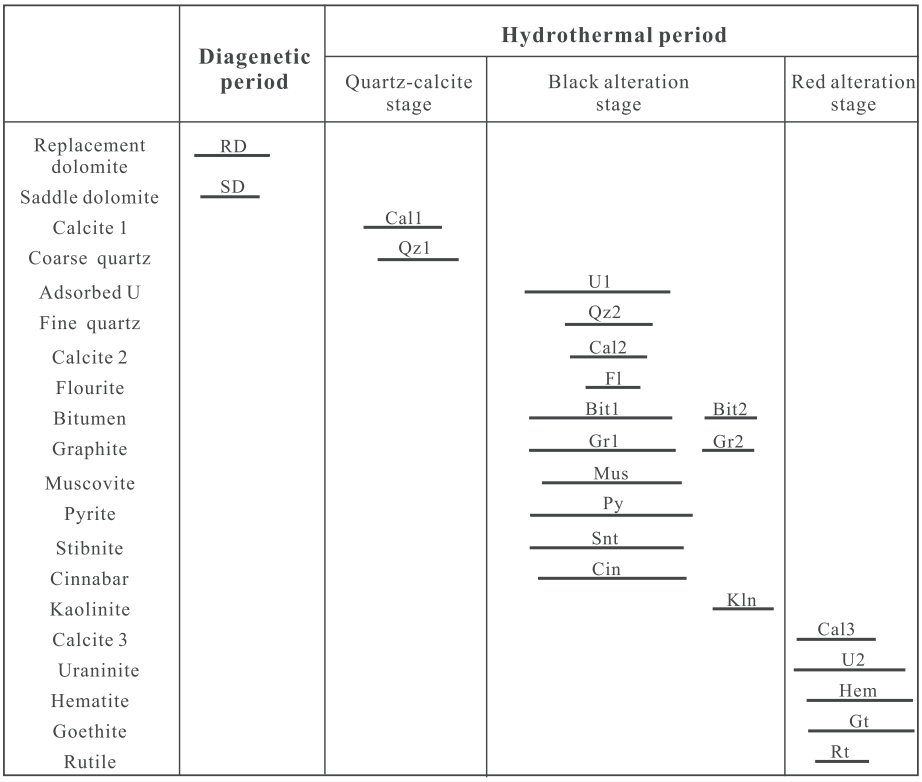

Fig. 8. Paragenetic sequence of minerals in the Baimadong deposit.

cinnabar, stibnite, hematite and goethite. The main gangue minerals are calcite, quartz, fluorite, kaolinite and muscovite.

3. Samples and study methods

Representative samples of the black-altered, red-altered and least altered rocks as well as the fault breccias (Fig. 4) were collected from outcrops and drill cores in the Baimadong uranium deposit for petrographic and geochemical studies. The sampling is focused on the black and red alterations, and the sample locations are shown in Fig. 1b. Whole rock samples were crushed and milled to powders for inorganic and organic geochemical analyses, and polished thin sections were made for petrographic and mineralogical observations. Densities of selected black-altered, red-altered and least altered rocks were

Table 1
The concentrations of major elements (%) and trace elements (ppm) of altered rocks from the Baimadong uranium deposit.

Sample	D20-2	D20-4	D23	D25	D26-1	D20-3	D26-2	D26-3	D20-1	D22-1	D22-2	D23-1	D26-4	D31	D29	D30
	Black-altered rocks						Red-altered rocks						Least altered rocks			
SiO_2	42.87	61.99	47.83	81.98	67.72	31.76	87.87	55.08	38.00	56.11	64.35	85.09	9.77	4.70	4.07	3.00
Al_2O_3	11.36	17.53	14.78	12.69	20.20	8.44	6.36	14.17	7.68	5.02	17.74	9.67	3.77	0.99	3.00	1.00
FeO^T	2.17	5.24	6.88	0.59	3.29	2.45	2.56	21.62	2.11	3.70	6.33	0.75	2.10	1.05	2.18	3.01
MgO	10.72	1.83	3.56	0.72	0.68	0.34	0.30	0.65	11.82	0.48	1.88	0.60	23.68	19.10	24.55	27.30
CaO	27.61	8.47	19.30	0.06	0.02	0.13	0.07	0.14	38.69	27.42	7.06	0.05	58.47	73.40	65.28	62.90
Na_2O	0.06	0.09	0.17	0.10	0.09	0.32	0.05	0.09	0.08	0.06	0.04	0.17	–	–	0.06	–
K_2O	2.21	1.93	2.53	1.64	2.17	0.54	0.79	1.66	0.64	0.71	0.79	1.76	0.36	0.12	0.15	0.38
P_2O_5	0.16	0.45	0.26	0.06	0.07	0.09	0.06	0.35	0.15	0.03	0.36	0.09	0.04	0.10	0.05	0.02
SO_3	2.19	1.45	3.40	1.13	4.89	20.08	0.61	2.11	0.08	5.79	0.09	0.62	0.26	0.11	0.18	1.78
TiO_2	0.22	1.02	0.84	0.52	0.33	0.31	0.23	0.58	0.23	0.58	0.20	0.62	0.09	0.10	0.13	0.08
TIC	21.75	–	0.24	0.00	0.12	–	0.24	0.12	23.57	9.48	25.97	0.18	40.27	45.78	39.36	40.12
U	3.99	3.82	5.33	7.90	9.70	4.16	7.21	15.88	3.03	5.72	3.24	5.89	0.67	0.86	0.77	0.73
Bi	0.08	0.08	0.40	0.17	0.28	0.04	0.11	0.29	0.10	0.24	0.07	0.23	0.06	0.30	0.13	0.09
Co	7.89	7.71	6.03	0.76	1.99	3.64	0.24	8.37	7.74	7.66	4.90	0.78	0.53	0.84	0.64	0.58
Cr	17.04	28.05	44.84	29.33	47.27	20.14	40.75	76.31	16.54	55.93	19.20	34.68	5.28	5.39	5.33	5.27
Cs	1.44	3.68	4.39	3.32	3.12	1.81	2.03	5.82	1.30	5.35	2.42	3.68	0.07	0.02	0.03	0.05
Cu	5.56	7.19	18.18	2.97	9.48	5.45	8.09	31.47	5.51	15.64	2.58	3.27	0.32	1.89	0.56	0.83
Ga	9.30	18.59	15.59	26.09	63.58	12.07	153.42	28.44	8.25	8.88	2.10	25.55	0.11	0.14	0.09	0.12
Hf	4.22	4.13	5.57	4.15	2.30	7.33	1.95	3.49	5.67	6.37	14.08	4.74	0.01	0.02	0.03	0.01
Li	12.57	21.12	32.15	43.15	23.40	12.33	26.06	49.16	10.72	28.03	6.43	24.74	0.91	0.95	0.92	0.94
Mn	126.26	129.83	35.37	23.70	16.62	136.26	12.35	29.55	136.74	540.9	104.55	19.68	154.99	133.44	132.33	140.11
Nb	5.09	7.74	11.07	12.17	7.86	7.51	5.39	13.12	5.69	11.53	5.44	14.59	0.06	0.06	0.05	0.06
Ni	16.88	17.34	13.55	2.04	5.47	9.50	0.38	27.20	15.48	30.18	8.15	1.76	6.16	8.08	6.49	7.87
Pb	16.86	19.26	30.45	27.41	34.44	14.52	12.88	49.53	17.57	20.39	4.61	20.21	0.10	0.69	0.50	0.33
Rb	27.90	65.98	39.27	37.20	26.15	47.71	16.38	48.75	21.19	18.39	10.24	46.17	0.15	0.18	0.16	0.15
Sc	4.23	7.86	2.92	4.04	2.28	4.77	1.62	8.28	4.03	10.89	4.04	2.83	0.13	0.20	0.18	0.15
Sn	0.54	1.09	3.09	2.01	1.45	0.68	0.98	2.84	0.63	2.37	0.61	2.77	0.00	0.09	0.03	0.01
Sr	97.92	131.55	237.08	165.57	179.84	81.62	216.34	145.71	107.97	750.06	214.08	245.93	41.19	51.00	45.32	47.09
Ta	0.43	0.67	0.99	1.03	0.68	0.68	0.45	1.12	0.47	0.93	0.45	1.25	0.02	0.03	0.02	0.01
Th	5.67	11.28	15.82	5.54	9.24	10.22	8.33	15.37	6.27	11.90	7.09	12.76	0.06	0.06	0.06	0.05
Ti	1302.76	1976.66	3068.82	3120.07	1992.05	1883.58	1379.02	3463.33	1396.00	3454.37	1171.41	3726.62	0.09	0.00	0.02	0.04
V	25.53	35.66	57.33	48.88	57.98	20.54	52.68	127.87	32.54	88.78	32.03	49.44	0.38	0.23	0.35	0.33
W	0.42	0.65	3.81	2.05	2.63	0.59	1.54	7.23	0.47	5.14	0.61	4.48	0.10	0.07	0.09	0.08
Zn	109.09	165.55	8.48	10.35	7.04	107.65	5.23	54.05	159.31	44.00	5.86	7.64	0.73	2.66	2.45	0.93
Zr	162.55	150.73	201.12	153.29	87.89	274.23	71.42	128.91	227.84	247.95	546.28	176.15	0.66	0.78	0.61	0.74
Ba	458.37	938.19	535.58	1299.48	3891.10	654.36	10056.83	1242.40	384.92	156.12	33.56	1284.15	5265.41	103.19	98.30	85.11
La	11.54	27.74	40.43	38.66	28.88	17.77	21.65	28.00	11.60	36.28	18.10	29.81	8.83	6.47	5.10	4.80
Ce	21.60	54.88	81.94	62.43	49.06	33.40	41.50	52.00	22.70	72.71	38.15	55.41	16.82	11.20	7.32	6.40
Pr	2.71	6.39	9.75	5.81	5.26	4.27	4.81	6.08	2.83	8.73	4.55	6.24	1.93	1.30	0.82	0.77
Nd	10.73	24.24	34.13	16.94	18.27	16.78	16.40	22.11	10.61	32.88	18.61	22.85	6.78	5.06	4.13	2.87
Sm	2.18	4.18	5.37	2.45	3.44	3.29	4.51	3.93	2.22	6.49	3.75	3.83	1.23	1.01	0.80	0.60
Eu	0.47	0.79	0.79	0.52	0.89	0.57	0.78	0.76	0.48	1.27	0.60	0.76	0.24	0.26	0.22	0.11
Gd	1.93	3.60	3.67	2.03	3.05	2.78	2.67	2.58	1.99	6.26	3.45	2.76	1.04	1.11	0.81	0.49
Tb	0.32	0.52	0.46	0.27	0.20	0.42	0.20	0.32	0.34	0.89	0.57	0.37	0.12	0.19	0.15	0.08
Dy	1.89	2.99	2.41	1.62	1.03	2.62	0.84	1.66	1.98	5.28	3.38	2.00	0.83	1.04	0.60	0.49
Ho	0.36	0.58	0.44	0.32	0.20	0.49	0.17	0.29	0.37	1.01	0.63	0.38	0.15	0.20	0.13	0.10
Er	1.09	1.68	1.40	1.03	0.63	1.50	0.50	0.99	1.16	2.88	1.92	1.24	0.42	0.58	0.30	0.29
Tm	0.19	0.27	0.24	0.19	0.13	0.24	0.10	0.19	0.19	0.46	0.32	0.22	0.07	0.11	0.05	0.05
Yb	1.27	1.76	1.62	1.27	0.74	1.63	0.53	1.26	1.24	2.97	2.07	1.55	0.44	0.55	0.32	0.29
Lu	0.20	0.26	0.26	0.20	0.12	0.27	0.11	0.19	0.20	0.46	0.33	0.24	0.05	0.08	0.06	0.05
Total REE	56.48	129.88	182.91	133.74	111.90	86.03	94.77	120.36	57.91	178.57	96.43	127.66	38.95	29.16	20.81	17.39
LREE/HREE	6.79	10.14	16.42	18.30	17.34	7.65	17.51	15.09	6.75	7.84	6.61	13.57	11.48	6.55	7.60	8.45
δEu	0.70	0.62	0.54	0.71	0.84	0.58	0.69	0.73	0.70	0.61	0.51	0.71	0.65	0.75	0.84	0.62
δCe	0.93	0.99	0.99	1.00	0.96	0.92	0.98	0.96	0.95	0.98	1.01	0.98	0.98	0.93	0.86	0.80

Notes: $\delta Eu = Eu_N/sqrt(Sm_N*Gd_N)$; $\delta Ce = Ce_N/(La_N*Pr_N)$; N = Chondrite normalized; TIC = Total inorganic carbon; "–" means no data.

measured for mass balance calculation.

Petrographic study was conducted on 93 polished thin sections using an Olympus BX51 petrographic microscope equipped with transmitted and reflected lights as well as UV fluorescence auxiliaries. A JEOL JSM-6360 scanning electron microscope (SEM) equipped with a Thermo Scientific Noran System 7 energy-dispersive spectroscopy (EDS), and a Renishaw RM2000 Raman spectroscopy with an excitation laser wavelength of 514 nm, were used as auxiliary tools to identify and characterize the black materials and fine-grained minerals. These petrographic analyses were carried out at the Geofluids Lab, University of Regina.

Whole rock composition analyses were carried out at the Sichuan Province Key Laboratory of Geoscience Nuclear Technology, Chengdu University of Technology. Major elements were analyzed using a wavelength-dispersive X-ray fluorescence spectrometry (XRF, PW2404) and following the procedure described by Norrish and Hutton (1969), with precision and accuracy better than 5%. Trace elements were conducted using an American Perkin Elmer type Elan DRC-e inductively coupled plasma mass spectrometer (ICP-MS), with precision and accuracy better than 10%.

Total inorganic carbon (TIC) was analyzed at Chengdu Mineral Resources Supervision and Testing Center of the Ministry of Land and Resources, using a LECO model CS230 combustion furnace instrument (LECO Corporation, St. Joseph MI) and a modified ASTM D153 method. Total organic sulfur (TOS), total organic carbon (TOC), and $\delta^{13}C_{org}$ of kerogen were measured at the Experimental Research Center of Wuxi

Table 2
The concentrations of TOC (%), TOS (%), δ^{13}Corg (‰) and chloroform asphalt "A" (ppm) as well as group components (%) and selected biomarker parameter of altered rocks from the Baimadong uranium deposit.

Sample	D20-2	D20-4	D23	D25	D26-1	D20-3	D26-2	D26-3	D20-1	D22-1	D22-2	D23-1	D26-4	D31	D29	D30
	Black-altered rocks						Red-altered rocks						Least altered rocks			
TOC	0.27	0.20	0.27	0.46	0.25	0.27	0.15	0.21	0.07	0.10	0.32	0.46	0.08	0.03	0.02	0.03
TOS	0.54	1.64	2.58	0.47	0.89	0.51	0.17	0.03	0.06	0.02	0.61	0.10	0.05	0.01	0.03	0.05
$\delta^{13}C_{org}$	− 29.60	− 29.60	− 28.00	− 27.40	− 28.00	− 29.70	− 25.50	− 27.70	− 28.20	− 25.00	− 26.60	− 28.50	− 26.60	− 27.00	− 27.60	− 27.30
Chloroform asphalt "A"	85.00	71.00	–	59.00	33.00	84.00	42.00	–	112.00	126.00	95.00	–	110.00	45.00	29.00	60.00
Saturated hydrocarbon	59.62	59.09	–	58.62	57.50	66.00	44.80	–	35.19	55.56	45.22	–	27.17	32.04	28.57	34.65
Aromatic hydrocarbon	5.16	5.05	–	4.83	8.75	8.00	29.60	–	3.70	5.05	16.56	–	4.62	4.85	7.79	3.94
Non-hydrocarbon + asphaltene	35.21	35.86	–	36.55	33.75	26.00	25.60	–	61.11	39.39	38.22	–	68.21	63.11	63.64	61.42
Pr/Ph	0.87	0.86	–	0.85	0.84	0.66	0.69	–	0.72	0.81	0.73	–	0.72	0.88	0.59	0.71

Abbreviation: TOC = Total organic carbon; TOS = Total organic sulfur; Pr = Pristane; Ph = Phytane; "–" means no data.

Petroleum Geology Research Institute, SINOPEC Petroleum Exploration and Production Research Institute. TOS and TOC were measured with a Leco CS-200 infrared carbon sulfur analyzer instrument. $\delta^{13}C_{org}$ were measured with a Finngan MAT-252 isotope mass spectrometer, following the technique of Deines and Wickman (1973), with the accuracy of ± 0.1‰ for delta values referencing to the V-PDB standard.

Chloroform asphalt "A" values of organic matter were obtained using a Soxhlet apparatus at the State Key Laboratory of Organic Geochemistry, Guangzhou Institute of Geochemistry, Chinese Academy of Sciences. The samples were pretreated using dilute HCI to wash the surface, and then the residual acid was washed away by water. In order to prevent partial loss and deterioration of organic matter caused by overheating with crusher instrument, all the samples were manually pulverized to 200 mesh with mortar, and then subjected to Soxhlet extraction using $CHCl_3$ (Trichloromethane) for 72 h. Group components were analyzed using silica gel and alumina column chromatography. Saturated hydrocarbons, aromatic hydrocarbons and non-hydrocarbons were obtained by using n-hexane, benzene and absolute ethanol as rinsing agents. Saturated hydrocarbon gas chromatography-mass spectrometry (GC-MS) was performed with a ThermoTRACE ULTRA-DSQIIinstrument. The oven temperature gradient was programmed from 60 °C to 300 °C at 4 °C/min, followed by an isothermal period of 15 min. Helium was used as carrier gas. The injector temperature (Int) is 300 °C, using HP-5MS silica capillary (60 m × 0.32 mm × 0.25 μm) as column.

Density measurements of rocks were done using a procedure modified from International Society for Rock Mechanics (1972) and Xiong (2006), as explained in detail by Chu et al. (2015). The isocon method proposed by Grant (1986), which is based on Gresens' (1967) theory, was used to estimate elements gained and lost during the alteration processes, as also explained in Chu et al. (2015).

4. Results

4.1. Petrography and paragenesis

The least altered rocks (Fig. 4a) consist mainly of dolomite (Fig. 5a), with variable amounts of detrital grains (dominantly quartz). In the black-altered rocks, which occur massively (Fig. 3) or in the matrix of breccias (Fig. 4e), the black material fills interstitial space (Fig. 5b) or fractures (Fig. 5c). In addition to detrital quartz, many of the quartz grains in black-altered rocks appear to be authigenic, as reflected by the well-developed crystal shapes (Fig. 5d). In the red-altered rocks, which appear to crosscut (Fig. 3) or overprint (Fig. 4d) the black-altered rocks, the reddish material is pervasively developed (Fig. 5e) or occurs as fracture fillings (Fig. 5f).

Saddle dolomite occurs as coarse crystals filling cavities or replacing earlier, relatively fine-grained replacement dolomite. The dolomites are brecciated and cemented by calcite (Cal 1) (Fig. 4f), and locally replaced by coarse-grained quartz (Qz 1) (Fig. 6a). Qz 1 is crosscut by black material (Black 1) (Fig. 6b and c) locally associated with calcite (Cal 2), which is in turn crosscut locally by veins of black material (Black 2) associated with kaolinite (Fig. 6d). Raman spectra suggest that the black material is composed of bitumen (Fig. 7a), which is fluorescent under UV excitation, and graphite (Fig. 7b), which is no-fluorescent. Pyrite is commonly found in the black material (Black 1), and occurs as disseminations or aggregates (Fig. 6e). Stibnite (Fig. 6f) and cinnabar also coexist with pyrite in the black material. Fluorite is locally developed in the black-altered rocks. The reddish material in the red-altered rocks (Fig. 5e and f) consists mainly of hematite and goethite, as confirmed by Raman spectroscopy (Fig. 7c and d). Minor amounts of rutile as well as calcite (Cal 3) are associated with the reddish material (Fig. 5f).

Based on the crosscutting relationships described above, the authigenic minerals in the Baimadong deposit are divided into two periods, i.e., the diagenetic period and the hydrothermal period, with the latter

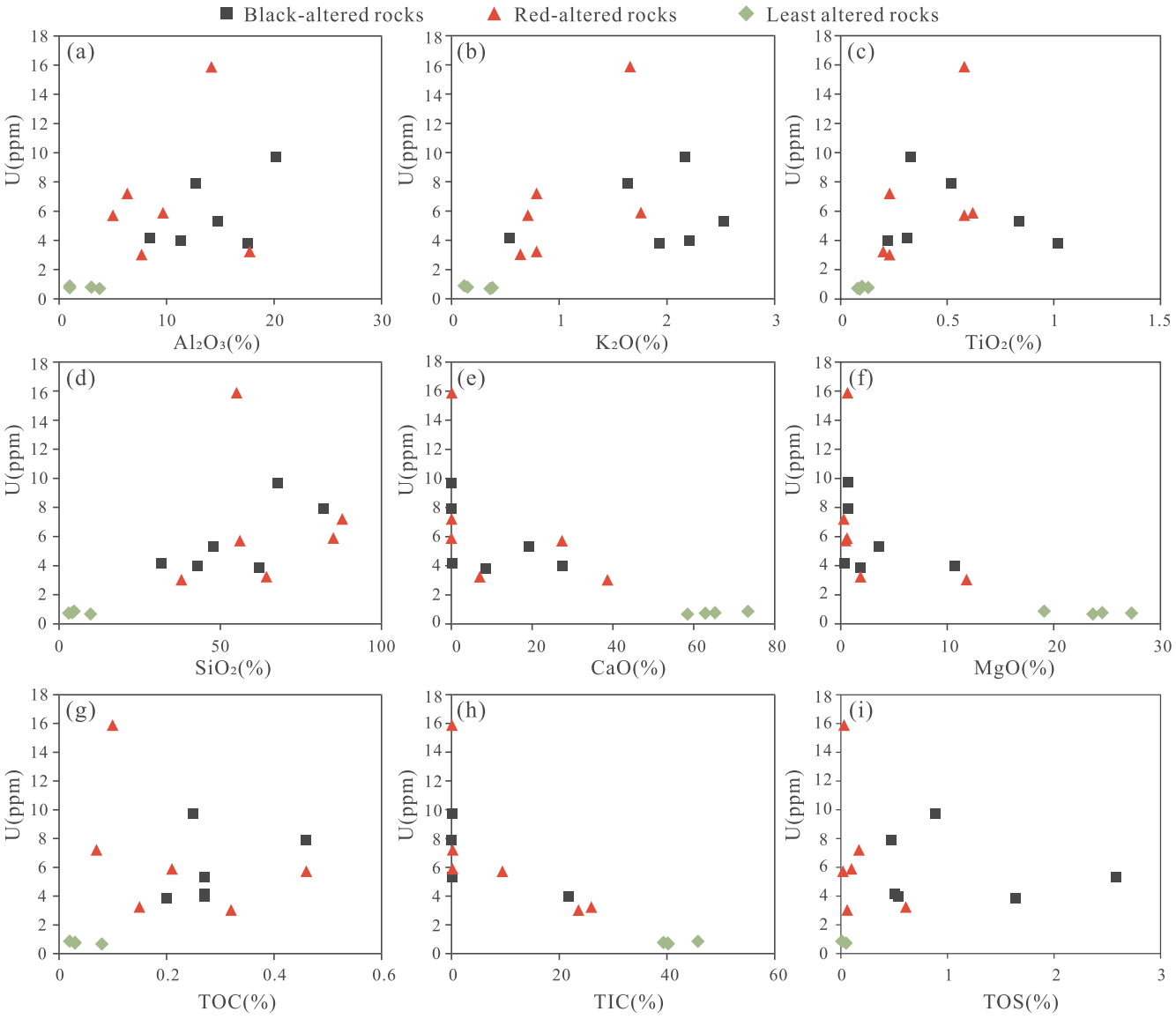

Fig. 9. Bivariant diagrams between various components in the least altered, black-altered and red-altered rocks of the Baimadong uranium deposit (data from Table 1). (a) U versus Al_2O_3; (b) U versus K_2O; (c) U versus TiO_2; (d) U versus SiO_2; (e) U versus CaO; (f) U versus MgO; (g) U versus TOC; (h) U versus TIC; (i) U versus TOS.

further divided into a quartz-calcite stage, black alteration stage, and red alteration stage (Fig. 8). Replacement dolomite and saddle dolomite were formed during the diagenesis, whereas all the other minerals occurred during the hydrothermal period. The coarse-grained quartz replacing the saddle dolomite (Fig. 6a) and calcite cementing dolomite breccias (Fig. 4f) are assigned to the quartz-calcite stage before the black alteration. The black material, which is made of bitumen and graphite and assigned to the black alteration stage, is divided into two sub-stages, labeled as Bit 1 – Gr 1 and Bit 2 – Gr 2. The bulk of the black material is made of Bit 1 and Gr 1, which are associated with fine-grained authigenic quartz (Qz 2), calcite (Cal 2), pyrite, stibnite, cinnabar and fluorite. The Bit 2 and Gr 2, which occur with kaolinite in veins (Fig. 6d), are minor components of the black material. Hematite, goethite, rutile and minor calcite (Cal 3) are assigned to the red alteration stage. Uraninite, although not observed in the samples examined in this study, is assigned to the red alteration stage (U2), based on previous petrographic, radiographic, α-track, electrodialysis and leaching test of the ores (Chen, 1990; Ni et al., 2012).

4.2. Whole rock geochemistry

Whole-rock major and trace elements data of three types of rocks are listed in Table 1 (TOC and TOS are given in Table 2). The black-altered rocks, red-altered rocks and least altered rocks have variable SiO_2 contents ranging from 31.76 to 81.98% (avg. = 55.69%, n = 6), 38.00 to 87.87% (avg. = 64.42%, n = 6) and 3.00 to 9.77% (avg. = 5.39%, n = 4), respectively. Other major components of the three types of rocks are also highly variable (Table 1), for example FeO^T = 0.59–6.88% (avg. = 3.44%) for black-altered rocks, 0.75–21.62% (avg. = 6.18%) for red-altered rocks, and 1.05–3.01% (avg. = 2.09%) for least altered rocks.

The three types of rocks also have variable concentrations of trace elements (Table 1). Notably the uranium concentrations in black-altered rocks (U = 3.99–9.70 ppm, avg. = 5.82 ppm) and red-altered rocks (U = 3.03–15.88 ppm, avg. = 6.83 ppm) are significantly higher than those of the least altered rocks (U = 0.67–0.86 ppm, avg. = 0.76 ppm). U concentrations appear to be positively correlated with Al_2O_3, K_2O, TiO_2, SiO_2, TOC and TOS, and negatively correlated with CaO, MgO and TIC (Fig. 9), which are consistent with the field and

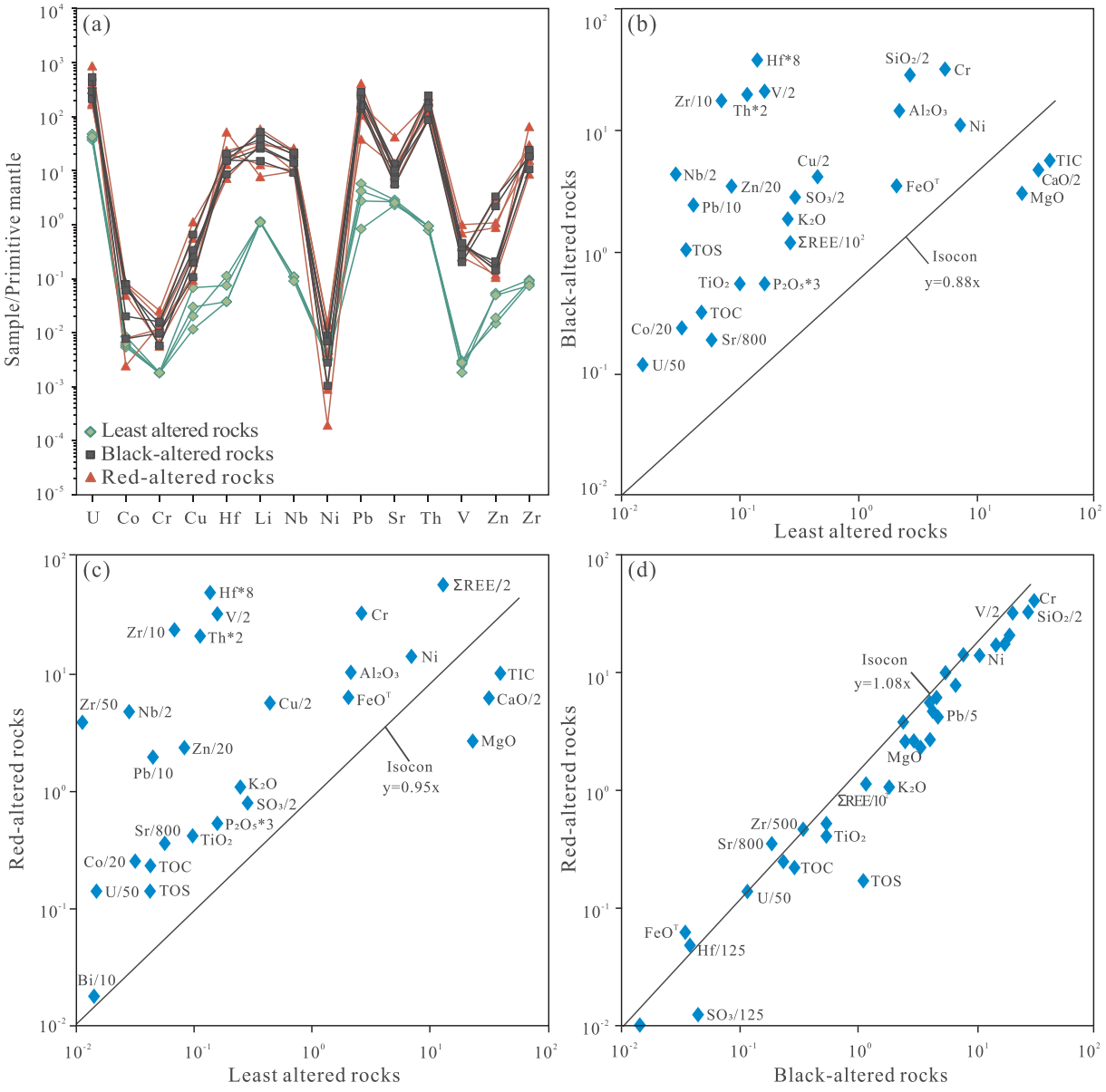

Fig. 10. (a) Primitive mantle-normalized spider diagrams of black-altered, red-altered and least altered rocks. Normalizing values are from McDonough and Sun (1995). (b–d) Isocon plots of various major and trace elements for black-altered versus least altered rocks (b), red-altered versus least altered rocks (c), and black-altered versus red-altered rocks (d). Note many elements have been scaled by *n for clarity.

microscopic observations that uranium mineralization is related to the black alteration, red alteration, silicification and argillization, as well as the development of sulfides in the black-altered rocks.

A comparison of the concentrations of trace elements among the three types of rocks indicates that both the black-altered and red-altered rocks are significantly enriched in most trace elements (e.g. U, Pb, Th, Zr) relative to the least altered rocks (Fig. 10a). The isocon diagrams (Grant, 1986) were constructed to evaluate the elements gained and lost during the black and red alterations (Fig. 10b–d). The isocons were constructed based on the assumption that the change of the volume of the rocks before and after the alterations was negligible, thus the slope of the isocons was determined by the change of the rock densities, which were measured to be 2.21–2.38 g/cm^3 (avg. = 2.30 g/cm^3) for the black-altered rocks, 2.24–2.70 g/cm^3 (avg. = 2.47 g/cm^3) for the red-altered rocks, and 2.51–2.68 g/cm^3 (avg. = 2.60 g/cm^3) for the least altered rocks. It is shown that most of the major elements and all of the trace elements measured in this study (Table 1), except CaO, MgO and TIC, were gained during the alteration from the least altered rocks to the black-altered rocks (Fig. 10b) or the red-altered rocks (Fig. 10c). However, most of the elements were neither gained nor lost during the alteration from the black-altered rocks to the red-altered rocks, except for the significant gained of TOC and TOS (Fig. 10d).

The three types of rocks display similar chondrite-normalized REE patterns, which are characterized by light rare earth elements (LREE) enrichment relative to heavy rare earth elements (HREE), and negative Eu anomalies (Fig. 11). The total rare earth elements (REE) concentrations in the black-altered rocks (56.48–182.91 ppm, avg. = 116.82 ppm) and red-altered rocks (57.91–178.57 ppm, avg. = 112.62 ppm) are much higher than those in the least altered rocks (17.39–38.95 ppm, avg. = 26.58 ppm). The LREE/HREE ratios are 6.79–18.30 (avg. = 12.77), 6.61–17.51 (avg. = 11.23), 6.55–11.48 (avg. = 8.52), the δEu values are 0.54–0.84 (avg. = 0.67), 0.51–0.73 (avg. = 0.66), 0.62–0.84 (avg. = 0.72), and the δCe values are 0.92–1.00 (avg. = 0.97), 0.95–1.01 (avg. = 0.98) and 0.80–0.98 (avg. = 0.89), for the black-altered, red-altered and least altered rocks, respectively.

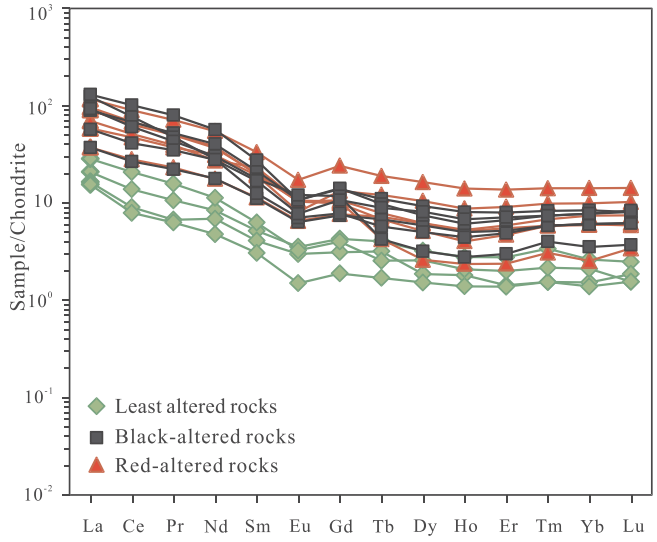

Fig. 11. Chondrite-normalized REE distribution patterns of black-altered, red-altered and least altered rocks. Normalizing values are from Sun and McDonough (1989).

4.3. Organic geochemistry

The total organic sulfur (TOS), total organic carbon (TOC) of the whole rocks, $\delta^{13}C_{org}$ values of the kerogen as well as the chloroform asphalt "A", selected biomarker parameter and group components of organic matter are listed in Table 2. TOS values range from 0.47 to 2.58% (avg. = 1.11%) for the black-altered rocks, from 0.02 to 0.61% (avg. = 0.17%) for the red-altered rocks, and from 0.01 to 0.05% (avg. = 0.04%) for the least altered rocks. TOC values range from 0.20 to 0.46% (avg. = 0.29%) for the black-altered rocks, from 0.07 to 0.46% (avg. = 0.22%) for the red-altered rocks and from 0.02 to 0.08% (avg. = 0.04%) for the least altered rocks. The black-altered rocks have the highest TOC and TOS values, whereas the least altered rocks are most depleted in TOC and TOS. Nevertheless, these types of rocks have similar $\delta^{13}C_{org}$ values of organic matter, e.g., from −29.7 to −27.4‰ for the black-altered rocks, from −28.5 to −25.0‰ for the red-altered rocks, and from −27.6 to −26.6‰ for the least altered rocks.

The black-altered, red-altered and least altered rocks also have similar contents of chloroform asphalt "A", but significantly different contents of saturated hydrocarbons, aromatic hydrocarbons as well as non-hydrocarbons and asphaltenes. The chloroform asphalt "A" contents of the black-altered rocks, red-altered rocks and least altered rocks range from 33 to 85 ppm (avg. = 66 ppm), 42 to 126 ppm (avg. = 94 ppm) and 29 to 110 ppm (avg. = 61 ppm), respectively. The saturated hydrocarbons contents range from 57.50 to 66.00% (avg. = 60.17%) for the black-altered rocks, 35.19 to 55.56% (avg. = 45.19%) for the red-altered rocks, and 27.17 to 34.65% (avg. = 30.61%) for the least altered rocks. The aromatic hydrocarbons contents range from 4.83 to 8.75% (avg. = 6.34%) for the black-altered rocks, 3.70 to 29.60% (avg. = 13.73%) for the red-altered rocks, and 3.94 to 7.79% (avg. = 5.30%) for the least altered rocks. The non-hydrocarbon + asphaltene contents range from 26.00% to 36.55% (avg. = 33.47%) for the black-altered rocks, 25.60 to 61.11% (avg. = 41.08%) for the red-altered rocks, and 61.42 to 68.21% (avg. = 64.10%) for the least altered rocks. These data indicate that the black-altered rocks are dominated with saturated hydrocarbons, followed by non-hydrocarbons and asphaltenes, and the red-altered rocks have a large proportion of saturated hydrocarbons and non-hydrocarbons + asphaltenes, whereas the least altered rocks have more non-hydrocarbons + asphaltenes than saturated hydrocarbons and aromatics.

In addition, the organic matters from the three types of rocks show similar biomarker characteristics. The gas chromatograms of n-alkanes fractions of all samples (Fig. 12) are characterized by n-alkanes between C_{13} and C_{28}, with a peak at C_{17} and prominent isoprenoids pristane (Pr) and phytane (Ph) singlet. The m/z191 mass fragmentograms of the saturated hydrocarbon fractions of all samples (Fig. 13) show high proportion tricyclic terpanes and low proportion pentacyclic terpane, however it is noticeable that the contents of pentacyclic terpane in the least altered rocks are higher than that in both the black-altered and red-altered rocks. The m/z217 ion chromatograms (Fig. 14) of all samples show similar distribution patterns with prominent diasteranes and steranes (C_{27}, C_{28} and C_{29}) peaks.

5. Discussion

5.1. Classification of the Baimadong uranium deposit

The Baimadong deposit has been classified as a carbonaceous-siliceous-pelitic rock-type uranium deposit (Hu et al., 2008; Zhang et al., 2009; Ni et al., 2012). On the other hand, because of its close association with the black-altered rocks, the Baimadong deposit is also assigned to the black rock series-type uranium deposits (Zhang et al., 2009; Ni et al., 2012), which are widespread in southwestern China (Tu, 1999; Ni et al., 2012). Furthermore, the Baimadong deposit was considered comparable to the black shale uranium deposits (Ni et al., 2012), although the black-altered rocks in this case are apparently not black shales.

In the 2018 IAEA classification, Baimadong is assigned to the carbonate-hosted deposits, along with 10 other deposits from Kyrgyzstan, India, USA and Mexico (IAEA, 2018), or more specifically, under the cataclastic carbonate type (IAEA, 2018). It has been noted that carbonate rocks are generally unfavorable host rocks for uranium mineralization because of their low permeability and lack of precipitation agents such as organic matter (IAEA, 2018), although high-permeability and organic-rich carbonate rocks are not uncommon, as manifested by development of oil and gas reservoirs in such type rocks. In the case of the Baimadong uranium deposit, the high permeability appears to be readily satisfied due to the development of the interformational fracture zones within the Qingxudong and Shilengshui formations adjacent to the Baimadong fault (Figs. 1b and 2), but the nature of organic matter in the black-altered rocks and its role in uranium mineralization need to be further discussed.

5.2. Source of organic matter in the black-altered rocks

The black material in the black-altered rocks is interpreted to be exogeneous based on the following observations: (1) organic matter is enriched in the altered zones in the mineralization area; (2) TOC values of the black-altered (and to a lesser extent, the red-altered) rocks are higher than those of the least altered rocks (Table 2); (3) macroscopic features indicate cross-formational nature of the black alteration (Fig. 3); and (4) the black material occurs in the matrix of the breccias (Fig. 4e) and as veinlets (Figs. 5c, 6c and d). Furthermore, the fluorescence of the bitumen under UV excitation suggests that the black material was originally petroleum (Shang et al., 1990), which was charged into the host rocks from external sources. This hypothesis is supported by the presence of petroleum inclusions in calcite in the Baimadong deposit (Chen, 1990).

The most possible source of the organic matter in the Baimadong deposit is the black shale of the Niutitang Formation (Figs. 1c, 2 and 15), as is supported by their similarity in organic geochemistry. The $\delta^{13}C_{org}$ values (−29.7 to −25.0‰) of the organic matter are comparable to sapropel-type (−30 to −27‰) rather than humus-type (−26.0 to –22.5‰) kerogen (Huang, 1984), suggesting that the organic matter is of marine origin, as also proposed for those from the Niutitang Formation (~ −31.51‰; Chen, 2005; Yang, 2009). The high contents of non-hydrocarbon + asphaltene components and low contents of

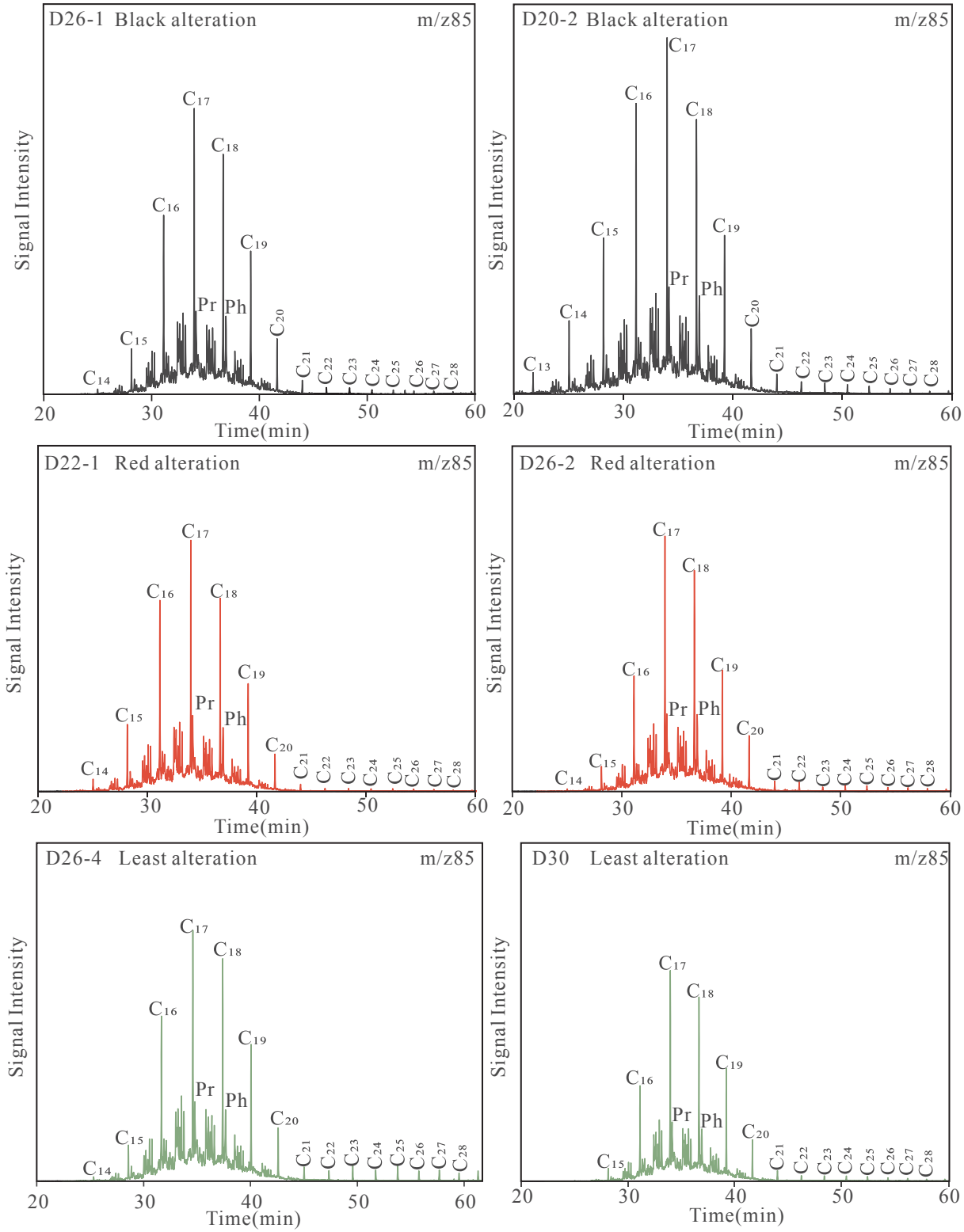

Fig. 12. The distributions of n-alkane *m/z* 85mass fragmentograms of saturated hydrocarbons of black-altered, red-altered and least altered samples from the Baimadong uranium deposit.

aromatic hydrocarbons (Table 2) are also consistent with aqueous rather than higher plants origin (Wen et al., 2000), as is the case for the black shale of the Niutitang Formation. The n-alkane distributions, characterized by predominance of low to medium molecular weight compounds (n-C_{13}–n-C_{28}) with a peak at C_{17} and without odd-even carbon number preference (Fig. 12), are indicative of marine algal origin of the organic matter (Clark and Blumer, 1967; Ebukanson and Kinghorn, 1986; Murray and Boreham, 1992), and so are the Pr/Ph ratios (0.66 to 0.87; Table 2) which are all < 1 (Philp, 1985; Amane and Hideki, 1997). The high contents of tricyclic terpanes (Fig. 13) and predominance of C_{27} (Fig. 14) further suggest that the source of organic matter is marine algal (Seifert and Moldowan, 1979; Huang and

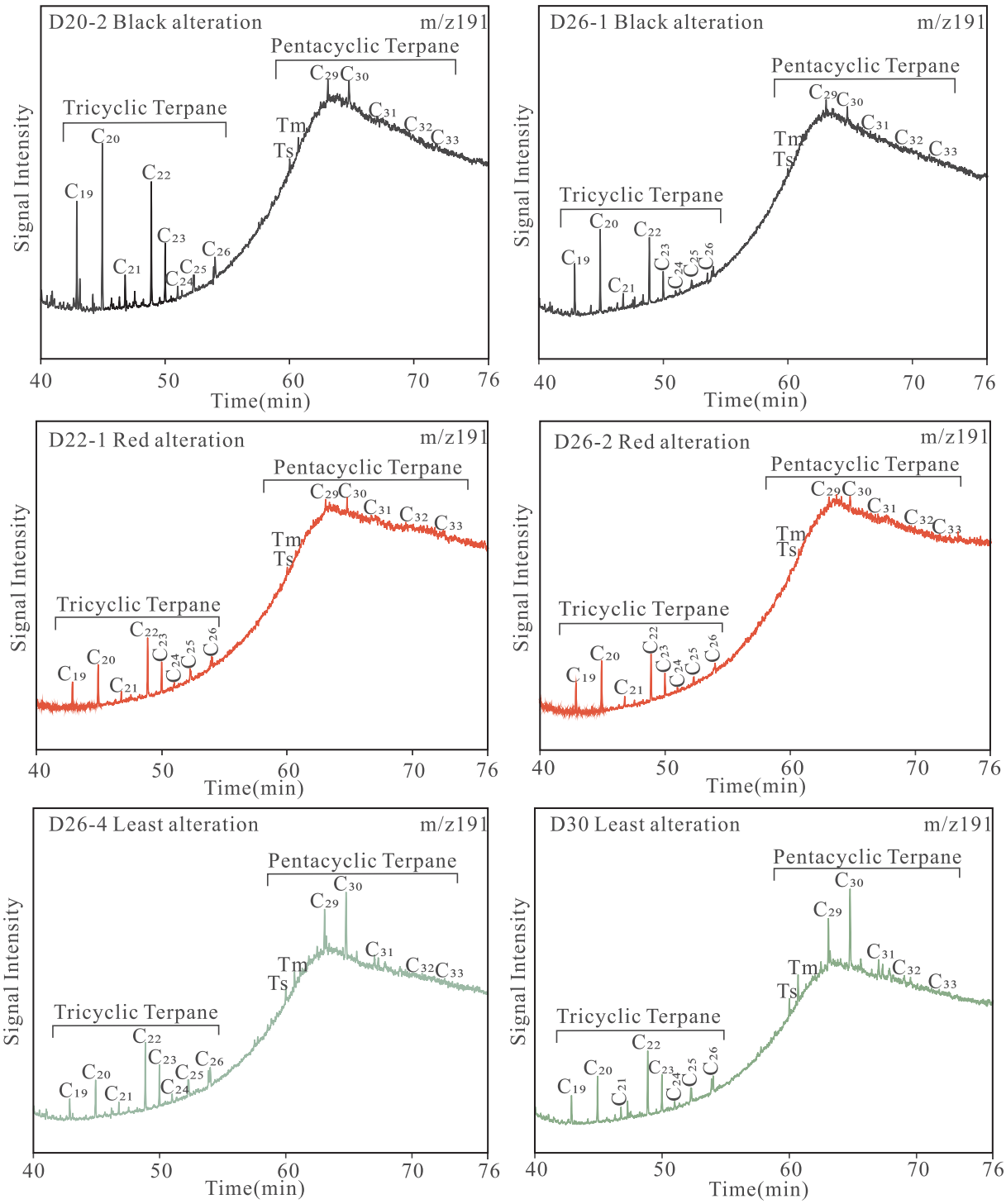

Fig. 13. The distributions of triterpanes *m/z* 191 mass fragmentograms of saturated hydrocarbons of black-altered, red-altered and least altered samples from the Baimadong uranium deposit.

Meinschein, 1979; Mackenzie, 1984). All these characteristics are comparable to those of the black shale of the Niutitang Formation (Chen, 2005).

The chloroform asphalt "A" contents of the altered rocks from the Baimadong deposit (29–126 ppm; Table 2) are also comparable to those of the black shale in the Niutitang Formation (16–193 ppm; Luo et al., 2014), which, together with the high Ro values (1.60–4.15%; Bai, 2012; Luo et al., 2014), indicate high degree of organic maturity. The organic matter in the Niutitang Formation in the studied region was subject to a long thermal history since the deposition in early Cambrian, reaching the dry gas stage in late Jurassic to early Cretaceous (Bai, 2012). Therefore, the Niutitang Formation is capable of supplying petroleum to the host rocks of the Baimadong deposit.

5.3. Ore-forming mechanism and relationship with the black and red alterations

The formation of uranium deposits generally results from reaction between oxidizing fluids carrying uranium and reducing agents, which reduces U^{6+} to U^{4+} and precipitates uranium minerals (Cuney and

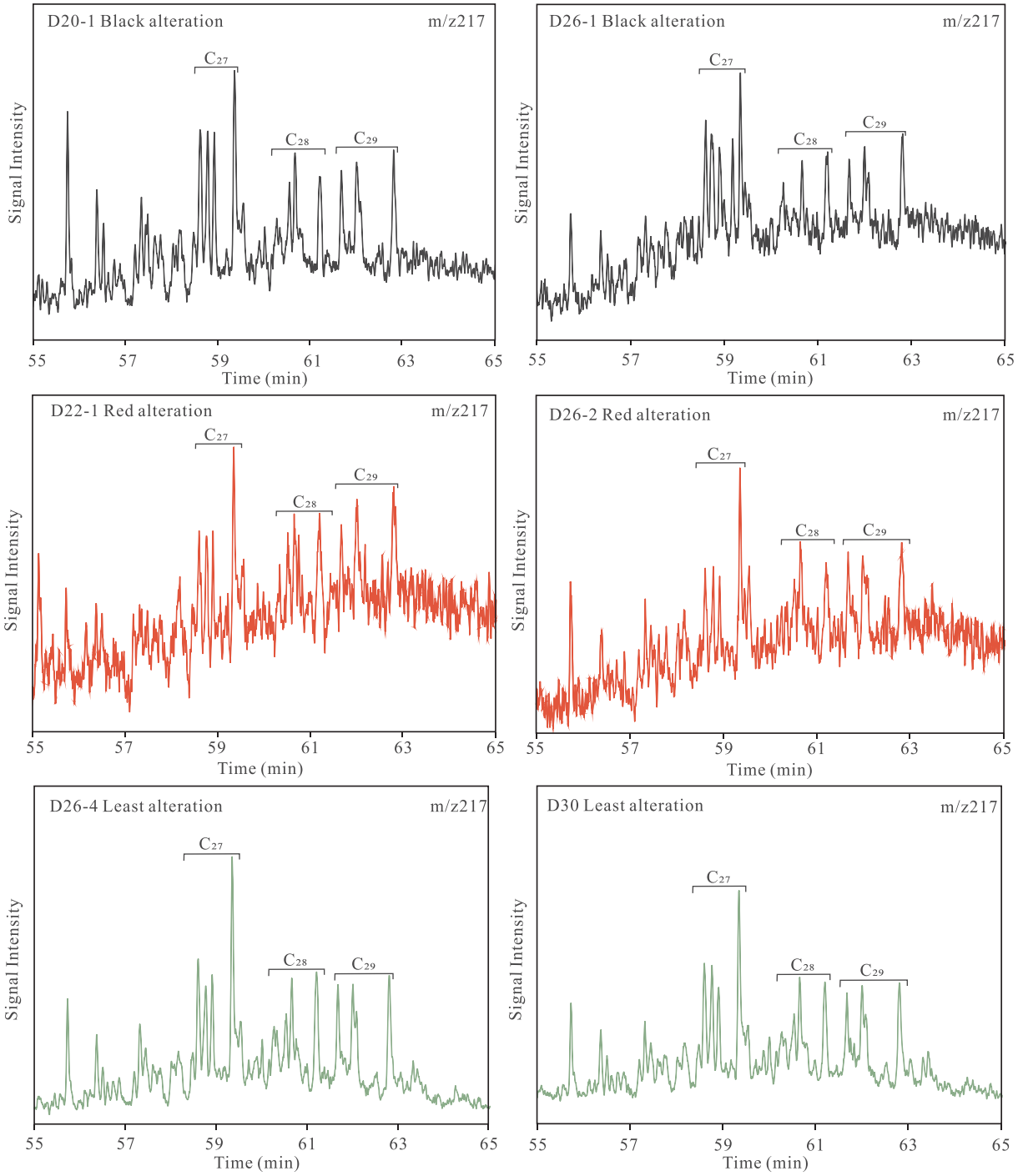

Fig. 14. The distributions of steranes *m/z* 217 mass fragmentograms of saturated hydrocarbons of black-altered, red-altered and least altered samples from the Baimadong uranium deposit.

Kyser, 2015; Feng et al., 2017). Based on the close spatial relationship between the uranium mineralization and the black and red alterations in the Baimadong deposit, it is proposed that the organic matter in the black alteration served as the main reducing agent, whereas the red alteration results from the redox reaction related to uranium mineralization, as illustrated in Fig. 15 and discussed.

It is difficult to determine the timing of petroleum migration from the Niutitang Formation to the carbonate rocks of the Qingxudong and Shilengshui formations. However, based on the close spatial relationship between the black alteration and the F1 fault in the Baimadong area, it is inferred that the main phase of petroleum charging may have occurred during the F1 normal faulting (Fig. 2), which most likely occurred in late Cretaceous to early Tertiary, when the study area and other parts of South China were under extensional tectonic regime due to the roll back of the subducted Pacific plate (Hu et al., 2008). The migration of petroleum was probably accompanied by hydrothermal fluids with high concentrations of silica, as reflected by strong silicification associated with the black alteration in the Baimadong area. Large amounts of gases, including CH_4, CO_2 and H_2S, may have been involved in this hydrothermal – hydrocarbon charging event, which may have led to crypto-explosion causing the formation of the breccia along the F1 fault (Figs. 1b, 2 and 15).

Preliminary uranium enrichment is inferred to have taken place during the black alteration, as reflected by the generally high U

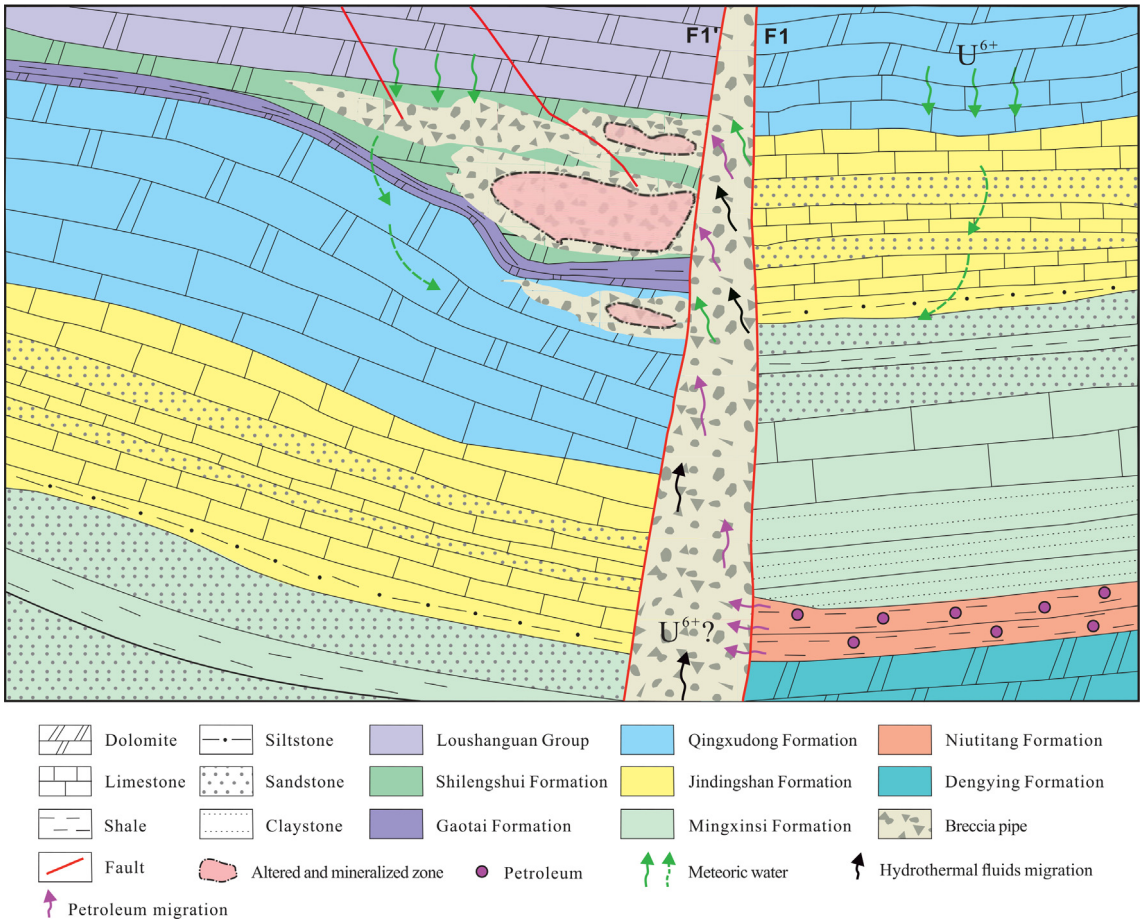

Fig. 15. Genetic model of the uranium mineralization of the Baimadong uranium deposit.

concentrations in the black-altered rocks. However, the nature of the fluid that carried uranium is uncertain. The black shale of the Niutitang Formation in South China is known to be enriched in multiple elements including U, Pb, Ni, Co, V, Mo, Cu, Au, Ag, Sb, Hg, PGE, REE, Se and P (Coveney and Nansheng, 1991; Li et al., 2003; Chen, 2005; Yang, 2009; Yang et al., 2013; Pi et al., 2013; Wang and Zhang, 2016; Zhang et al., 2017). Among them, the U concentrations of the Niutitang Formation is 10 times compared with that of crustal sedimentary rocks and 6 to 20 times compared with that of the crust (Ni et al., 2012). Most of these elements are also enriched in the black-altered rocks at the Baimadong deposit (Fig. 10a). It is attempting to envisage that the petroleum sourced from the Niutitang Formation may have carried significant amounts of U and associated elements in adsorption and fixed them in the black-altered rocks at Baimadong. However, this hypothesis is not supported by the observation that uranium is generally very low (< 5 ppb) in petroleum (Bell, 1960). Alternatively, a separate hydrothermal fluid carrying uranium and silica may have followed the same structure (F1 fault) as the petroleum migration, and they encountered each other at Baimadong, resulting in preliminary uranium enrichment, black alteration and silicification. The uranium may have been derived from various sources including the Niutitang Formation. It is notable that high concentrations of U have also been found in other strata, e.g., up to 12.4 ppm in the Sinian Dengying Formation (Yang et al., 2014). U may have been transported as F complexes as suggested by the association of fluorite with the black alteration.

Although black-altered rocks are enriched in uranium, the U concentrations are generally below ore grade. Based on the observation that orebodies are best developed where red alteration overprints the black-altered rocks, it is inferred that the main phase of uranium mineralization is related to a fluid event associated with the red alteration. The incoming fluid was most likely oxidizing and carrying U^{6+}, which reacted with the reducing agents in the black-altered rocks (organic matter, and to a lesser extent Fe^{2+} and sulfides) and precipitated uraninite. At the same time, Fe^{2+} was oxidized to Fe^{3+} and hematite as well as goethite were precipitated, causing the red alteration (Fig. 15).

The reddening and uranium mineralization event may be fairly young, based on the uraninite U-Pb ages of 27.8–28.9 Ma (Tang and Zhu, 1986) and 44.7–51.5 Ma (Chen, 1990). The H-O isotope data indicate that the ore-forming fluids in the Baimadong deposit have a dominantly meteoric source (Chen, 1990). The uranium may have been derived from various rocks that the meteoric fluid encountered in its path, including the U-rich Cambrian sedimentary rocks that may have been exposed on the surface elsewhere in the Qianzhong uplift (Long et al., 2018).

The overall extensional tectonic environment, plus enhanced permeabilities related to faulting and brecciation along the F1 fault, may have greatly facilitated the deep circulation of the meteoric water and extraction of uranium (Fig. 15). The black alteration played a critical role in the uranium mineralization, both as ground preparation (setting up a reducing environment and geochemical trap for mineralization) and as an initial uranium enrichment. However, these roles alone are not sufficient for economic uranium mineralization. It is the structural activity, particularly faulting along the F1 fault and adjacent interformational fracture zones, that controlled both the black alteration and subsequent uranium mineralization and eventually led to the formation of the deposit.

6. Conclusions

The Baimadong uranium deposit is hosted in carbonate rocks of the

Cambrian Qingxudong and Shilengshui formations, and is closely related to the black and red alterations. The black material in the black-altered rocks is made of graphite and bitumen, which was introduced into the host rocks, i.e., exogeneous rather than indigenous. Organic geochemical studies indicate that the black material was originally petroleum derived from the black shale of the Niutitang Formation underneath the deposit, which migrated along the F1 normal fault and was charged into adjacent interformational fracture zones. Uranium and multiple metals were preliminarily enriched during the black alteration, whereas the main phase of uranium mineralization took place during a subsequent fluid event associated with the red alteration that overprints the black alteration. Uranium was carried by an oxidizing fluid of meteoric origin, which reacted with the reducing agents in the black-altered rocks and precipitated uraninite, hematite and goethite. The black alteration was accompanied by preliminary uranium enrichment and created a reducing condition for subsequent main-phase uranium mineralization. Both the black alteration and overprinting red alteration were controlled by the same structural framework, which facilitated fluid circulation and ore precipitation. The structural control, together with red alteration overprinting black alteration, is an important factor to be considered in the exploration of this type uranium deposits.

Although the Baimadong uranium deposit is associated with black rocks which appear to resemble black shales, it is clearly different from black shale uranium deposits as defined by IAEA (2009, 2018), because the organic matter in the host rocks was derived from an external source. Furthermore, although the Baimadong uranium deposit may still be classified as the carbonaceous-siliceous-pelitic rock-type or black-rock type deposits, this is not recommended because the definition of these types of deposits are ambiguous. In contrast, it is unambiguous to classify Baimadong as a carbonate-hosted deposit or cataclastic carbonate deposit (IAEA, 2018), the latter also having the advantage of highlighting the importance of structural control.

Acknowledgements

This research was financially supported by the National Natural Science Foundation of China (Nos. 40872069 and 41272100). We would like to thank members of the Geofluids Group at the Department of Geology, University of Regina for stimulating discussion. The editor, associate editor and anonymous reviewers are thanked for their constructive comments that helped greatly improve the paper.

References

Amane, W., Hideki, N., 1997. Geochemical characteristics of terrigenous and marine sourced oils in Hokkaido, Japan. Org. Geochem. 28, 27–41.

Bai, Z.R., 2012.Sedimentary characteristics of the Lower Cambrian Niutitang Fm shale and evaluation parameters of shale gas in Zunyi-Qijiang area. A dissertation submitted for the degree of Doctor of Science of the China University of Geosciences, pp. 45–62 (in Chinese with English abstract).

Bell, K.G., 1960. Uranium and other trace elements in petroleums and rock asphalts. USGS Professional Paper 356-B, 65 p.

Chen, L., 2005. Sedimentology and geochemistry of the Early Cambrian black rock series in the Hunan-Guizhou area, China. A dissertation submitted for the degree of Doctor of Science of the Chinese Academy of Sciences and for the Diploma of the Institute of Geochemistry, pp. 53–79 (in Chinese with English abstract).

Chen, L.M., 1990. Discussion on the origin of uranium deposit NO. 504. Uranium Geol. 6, 135–144 (in Chinese with English abstract).

Chu, H., Chi, G., Bosman, S., Card, C., 2015. Diagenetic and geochemical studies of sandstones from drill core DV10-001 in the Athabasca basin, Canada, and implications for uranium mineralization. J. Geochem. Explor. 148, 206–230.

Clark, R.C., Blumer, M., 1967. Distribution of n-poraffines in marine organisms and sediment. Limnol. Oceanogr. 12, 79–87.

Coveney Jr., R.M., Nansheng, C., 1991. Ni-Mo-Au-rich ores in Chinese black shales and speculations on possible analogues in the United States. Miner. Deposi. 26, 83–88.

Cuney, M., Kyser, K., 2015. Geology and geochemistry of uranium and thorium deposits. Mineralogical Association of Canada, Short Course Series Volume 46, 345 p.

Dai, C.G., Chen, J.S., Lu, D.B., Ma, H.Z., Wang, X.H., 2010. Wuling orogeny in Eastern Guizhou and its adjacent regions and its geological significance. J. Geomech. 16, 78–84 (in Chinese with English abstract).

Deines, P., Wickman, F.E., 1973. The isotopic composition of 'graphitic' carbon from iron meteorites and some remarks on the troilitic sulfur of iron meteorites. Geochim. Cosmochim. Acta 1973, 1295–1319.

Ebukanson, E.J., Kinghorn, R.R.F., 1986. Maturity of organic matter in the Jurassic of southern England and its relation to the burial history of the sediments. J. Petrol Geol. 93, 259–280.

Feng, Z.B., Nie, F.J., Deng, J.Z., Zhang, H.J., Liu, B.H., 2017. Spatial-temporal collocation and genetic relationship among uranium, coal, and hydrocarbons and its significance for uranium prospecting: A case from the Mesozoic-Cenozoic uraniferous basins, North China. Russ. Geol. Geophys. 58, 611–623.

Grant, J.A., 1986. The isocon diagram- a simple solution to Gresen's equation for metasomatic alteration. Econ. Geol. 81, 1976–1982.

Gresens, R.L., 1967. Composition-volume relationships of metasomatism. Chem. Geol. 2, 47–55.

Guizhou Bureau of Geology and Minerals, 1987. Geological Marks of Guizhou Province. Geological Publishing House, Beijing, pp. 1–360 (in Chinese).

He, B., Xu, Y.G., Wang, Y.M., 2005. Nature of the Dongwu movement and its temporal and spatial evolution. J. China Univ. Geosci. 30, 89–96 (in Chinese with English abstract).

Hu, R.Z., Bi, X.W., Zhou, M.F., 2008. Uranium metallogenesis in South China and its relationship to crustal extension during the Cretaceous to Tertiary. Econ. Geol. 103, 583–598.

Huang, T.K., 1945. On major tectonic forms of China. Geol Memoirs Ser A. 20, 165.

Huang, S.X., Du, L.T., Xie, Y.X., Zhang, D.S., Chen, G., Wan, G.L., Ji, S.F., 1994. Uranium deposits in China. In: Song, S.H., Ed., Mineral Deposits in China, pp. 329–385.

Huang, D.F., Li, J.C., Zhang, D.J., 1984. Kergon types and study on effectiveness, limitation and interrelation of their identification parameters. Acta Sedimentol. Sin. 2, 18–33 (in Chinese with English abstract).

Huang, W.Y., Meinschein, W.G., 1979. Sterols as ecological indicators. Geochim. Cosmochim. Acta 43, 739–745.

Huang, K.P., Zheng, M.R., 2016. Geochemical characteristics and genesis of Baimadong uranium deposit in Guizhou. Miner. Resour. Geol. 30, 609–614 (in Chinese with English abstract).

IAEA, 2009. World distribution of uranium deposits (UDEPO) with uranium deposit classification. IAEA-TECDOC-1629, 117 p.

IAEA, 2018. Geological classification of uranium deposits and description of selected examples. IAEA-TECDOC-1842, 415 p.

International Society for Rock Mechanics (ISRM), Commission on standardization of laboratory and field tests, 1972. Suggested Methods for Determining the Slaking, Swelling, Porosity, Density and Related Rock Index Properties. Int. Soc. Rock Mech. secretary, Lisbon, pp.143–151.

Li, C.Y., Liu, Y.P., Ye, L., Pi, D.H., 2003. Discussion on some problems in the study of mineralization in Guizhou. Bulletin of Miner. Petrol. Geochem. 22, 350–355 (in Chinese with English abstract).

Ling, K.Y., Zhu, X.Q., Tang, H.S., Wang, Z.G., Yan, H.W., Han, T., Chen, W.Y., 2015. Mineralogical characteristics of the karstic bauxite deposits in the Xiuwen ore belt, Central Guizhou Province, Southwest China. Ore Geol. Rev. 65, 86–96.

Liu, X.Z., 1989. The main achievements and prospect for uranium geology work of China. Uranium Geol. 5, 257–267 (in Chinese with English abstract).

Liu, P., 2001. Discussion on the metallogenic setting of the Qianzhong-Yu'nan bauxite in Guizhou and its genesis. Guizhou Geol. 18, 238–243 (in Chinese with English abstract).

Long, Y.Z., Chi, G.X., Liu, J.P., Jin, Z.G., Dai, T.G., 2017. Trace and rare earth elements constraints on the sources of the Yunfeng paleo-karstic bauxite deposit in the Xiuwen-Qingzhen area, Guizhou, China. Ore Geol. Rev. 91, 404–418.

Long, Y.Z., Chi, G.X., Liu, J.P., Song, H., 2018. Uranium enrichment in a paleo-karstic bauxite deposit, Yunfeng, SW China: Mineralogy, geochemistry, transport-deposition mechanisms and significance for uranium exploration. J. Geochem. Explor. 190, 424–435.

Luo, C., Liu, S.G., Sun, W., Ran, B., Yong, Z.Q., Yang, D., Zhang, X., Wang, S.Y., Ye, Y.H., Deng, B., 2014. Basic characteristics of shale gas in the Lower Cambrian Niutitang Formation in the Upper Yangtze region: Taking Nangao Section in Danzhai as an example. Nat. Gas Geosci. 25, 453–467 (in Chinese with English abstract).

Mackenzie, A.S., 1984. Application of biomarkers in petroleum geochemistry. In: Welte, D., Brooks, J. (Eds.), Advances of Petroleum Geochemistry. Academic Press, pp. 115–214.

McDonough, W.F., Sun, S.S., 1995. The composition of the Earth. Chem. Geol. 120, 223–253.

Mei, M.X., Ma, Y.S., Deng, J., Li, H., Zheng, K.B., 2005. Tectonic palaeogeographic changes resulting from the Caledonian movement and the formation of the Dianqiangui Basin: discussion on the deep exploration potential of oil and gas in the Dianqiangui Basin. Earth Sci. Front. 12, 227–236.

Min, M., 1995. Carbonaceous-siliceous-pelitic rock type uranium deposits in Southern China: geological setting and metallogeny. Ore Geol. Rev. 10, 51–64.

Mo, B.H., Zhu, X.Y., Yao, Y.F., Sun, Z.X., Zhang, J., 2016. Analysis on uranium mineralization characteristics and ore-controlling factors of deposit 504. Guizhou. World Nucl. Geosci. 33, 19–25 (in Chinese with English abstract).

Murray, A.P., Boreham, C.J., 1992. Organic Geochemistry in Petroleum Exploration. Australian Geological Survey Organization, Canberra, pp. 1–230.

Ni, S.J., Xu, Z.Q., Zhang, C.J., Song, H., Luo, C., 2012. Uranium metallogenesis and ore genesis of the rich-large black rock series-type uranium deposits in Southwest China. Adv. Earth Sci. 27, 1035–1042 (in Chinese with English abstract).

Norrish, K., Hutton, J.T., 1969. An accurate X-ray spectrographic method for the analysis of a wide range of geological samples. Geochim. Cosmochim. Acta 33, 431–453.

Philp, R.P., 1985. Biolgical markers in fossil fuel production. Mass Spectrom. Rev. 4, 1–54.

Pi, D.H., Liu, C.Q., Shields-Zhou, G.A., Jiang, S.Y., 2013. Trace and rare earth element

geochemistry of black shale and kerogen in the early Cambrian Niutitang Formation in Guizhou province, South China: constraints for redox environments and origin of metal enrichments. Precambr. Res. 225, 218–229.
Seifert, W.K., Moldowan, J.M., 1979. The effect of biodegradation on steranes and terpanes in crude oils. Geochim. Cosmochim. Acta 43, 111–126.
Shang, H.Y., Li, J.C., Guo, S.L., 1990. Organic Geochemistry and Fluorescence Microscopy Technology. Petroleum Industry Press, Beijing.
Sun, S.S., McDonough, W.F., 1989. Chemical and isotopic systematics of oceanic basalts: implications for mantle composition and processes. In: Saunders, A.D., Norry, M.J. (Eds.), Magmatism in Ocean Basins. Geological Society of Special Publication, London, pp. 313–345.
Tang, J.R., Zhu, J.C., 1986. Metallogenetic chronology of certain stratabound uranium deposits, province Guizhou. Uranium Geol. 2, 349–352 (in Chinese).
Tu, G.Z., 1999. On the central Asia metallogenic Province. Chin. J. Geol. 34, 397–404 (in Chinese with English abstract).
Wang, H.Z., Mo, X.X., 1995. An outline of the tectonic evolution of China. Epis 18, 6–16.
Wang, S., Zhang, J., 2016. Mineral and rock composition and resource properties of lower Cambrian black shale in Zhijin, Guizhou Province. Acta Petrol. Miner. 3, 543–552 (in Chinese with English abstract).
Wen, H.J., Qiu, Y.Z., Yao, L.B., Lu, J.L., Peng, P.A., Lin, Q., 2000. Organic geochemistry and biomarkers of some Lower Cambrian high-selenium formations in China. Geochimica. 29, 28–35 (in Chinese with English abstract).
Xiong, W.Q., 2006. Application of electron balance to the block density tests by suspending weigh method. Chin. J. Geotech. Eng. 28, 793–795 (in Chinese with English abstract).
Yang, J., 2009. Study on the formation environment and geochemistry of Lower Cambrian black shale series, Northern Guizhou Province, China. A dissertation submitted for the degree of Doctor of Chang'an University, Xi'an, China, pp. 50–78 (in Chinese with English abstract).
Yang, E.L., Lu, X.B., Bao, M., Luo, J.J., Hu, Q.C., 2013. Enrichment and origin of some trace elements in black shales from the early Cambrian in eastern Guizhou Province. Adv. Earth Sci. 28, 1160–1169.
Yang, R.D., Ren, H.L., Liu, K., Gao, J.B., 2014. Geochemical characteristics of uranium mineralization rock in Baimadong. Kaiyang Country, Guizhou Province Geosci. 28, 905–914 (in Chinese with English abstract).
Yi, T.S., Zhao, X., 2014. Characteristics and distribution patterns of the Lower Cambrian Niutitang Shale reservoirs in Guizhou. China. Nat. Gas Ind. 34, 1–7 (in Chinese with English abstract).
Yu, K.F., Wang, S.D., 1995. Duyun movement in South Guizhou Province and its paleostructure, and their significance in petroleum geology. Uranium Geol. 12, 225–232 (in Chinese with English abstract).
Zhang, D., 1982. Contributions of the uranium deposits of carbonaceous-siliceous-argillaceous rock type in China. Atomic Energy Publishing House, Beijing, pp. 129–138 (in Chinese).
Zhang, Y.Z., 1995. Effect of Xuefeng orogeny in Tianzhu Region. Southeast Guizhou. Guizhou Geol. 13, 30–36 (in Chinese with English abstract).
Zhang, X.Q., Huang, K.P., Yuan, L., Shen, X.D., Zheng, M.R., 2017a. Prospecting potential analysis and uranium mineralization control of deep fracture and interlayer detachment structure system of Baimadong uranium deposit in Guizhou. Guizhou Geol. 34, 237–243 (in Chinese with English abstract).
Zhang, L., Liu, C., Fayek, M., Wu, B., Lei, K., Cun, X., Sun, L., 2017b. Hydrothermal mineralization in the sandstone–hosted Hangjinqi uranium deposit, North Ordos Basin. China. Ore Geol. Rev. 80, 103–115.
Zhang, C.J., Ni, S.J., Xu, Z.Q., Chen, Y.L., 2009. Preliminary study on major geological events and uranium mineralization in the Western margin of the Yangtze platform and adjacent areas. Acta Mineral. Sin. 648–649 (in Chinese).
Zhou, J.X., Huang, Z.L., Lv, Z.C., Zhu, X.K., Gao, J.G., Mirnejad, H., 2014. Geology, isotope geochemistry and ore genesis of the Shanshulin carbonate-hosted Pb-Zn deposit, southwest China. Ore Geol. Rev. 63, 209–225.